Chapter 4

Experimental Results and Discussion

In this chapter, there are two main topics are described. The first part is the magnetic results of magnetic films including of the thermal treatment of PtMn-based MTJ, and the Os diffusion barrier in the CoFe/OsMn systems. The second part is focused on the buffer layer use of Os in CoFe/IrMn systems and the growth of Os (0002) on different substrates.

4-1 Magnetic results of magnetic films

4-1-1 Thermal treatments of PtMn-based MTJ

After annealing roughly above 240°C, the structure of PtMn film will change from a disordered face center cubic (fcc) (111) to an ordered face center tetragonal (fct) (111) [109-111]. According to Kim et al [111], the optimal H_{ex} can be obtained for PtMn annealed at 270°C for 35 hours. However, very few studies have been focused on the effect of a short time annealing treatment as well as post-annealing after patterning for MTJ samples with PtMn layer. The purpose of this study is to indicate how the structure, magnetization and the interlayer coupling in MTJ system with PtMn layer varies with the annealing temperature and annealing time.

The MTJ samples were deposited on thermally oxidized Si substrates in a RF multi-target sputtering system. The sample structures were substrate/Ta/NiFe/PtMn (d)/CoFe/Ru/CoFe/Al_2O_3/CoFe/NiFe/Ta, with d = 8, 10, 12.5, 15, 17.5, and 20 nm. Fig. 4-1 shows the XRD patterns of the MTJ with d = 15 before and after 300°C annealing for 1 hour. The diffraction peak at 2θ = 40.1° represents PtMn fcc (111) structure, and peak at 2θ = 40.4° is for PtMn fct (111) structure. Such a temperature is slightly higher than the suitable

annealing temperature well-used in other studies. The phase change of PtMn was found obviously while the crystallinity of the CoFe was also gotten better. This shows clearly that the structure of the sample transformed from fcc (111) to fct (111) after annealing. The diffraction peak at $2\theta = 43.5°$ relates to fcc (111) for either CoFe or NiFe layers. Compared with other PtMn thickness, the shifts of the PtMn peak all indicated that the PtMn had phase changed, as shown in Fig. 4-2 (a). The full width at half maximum (FWHM) of PtMn and CoFe decreased as the PtMn increasing meant the degree of the crystallinity of each peak was more affected by the PtMn thickness. Thicker PtMn brought better crystallinity of PtMn and CoFe, thus, lower FWHM, as shown in Fig. 4-2 (b). After annealing, all peaks of PtMn and CoFe/NiFe got better crystallinity and the FWHM of these peaks all became lower that meant the peaks became stronger. However, MTJ with d = 8 showed slightly raised FWHM due to the process of PtMn phase change did not complete well.

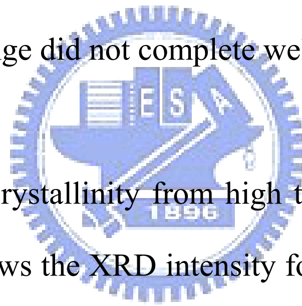

For avoiding damage in crystallinity from high temperature annealing, show annealing time was test first. Fig. 4-3 shows the XRD intensity for PtMn, CoFe/NiFe of as a function of diffraction angles for MTJ sample with d = 15 without and with annealing at 400°C for 10 minutes. Again, the results showed clearly that the structure of the sample transformed from fcc (111) to fct (111) even after annealing at 400°C for only 10 minutes. Like samples annealing with standard conditions, the atomic layer distance between two PtMn structures could be calculated, and it changes from 2.24 Å (fcc) to 2.22 Å (fct). Fig. 4-4 shows the PtMn peak-positions of MTJ samples as functions of annealing time and PtMn thickness. All samples showed PtMn phase changed even though the annealing time as short as 10 minutes except the sample with 8 nm PtMn. Figure 4-5 shows the peak intensities, the peak-positions, and the FWHM of peaks of PtMn and CoFe for samples with d varied from 8 to 20 nm after 400°C annealing for different annealing time. It was easily found that all short time 400°C annealing can make PtMn phase changed while the CoFe peaks get better crystallinity at the

same time. Both XRD intensity and FWHM of PtMn peak for samples with d varied from 8 to 20 nm and annealing at 400°C for 10 minutes and 1 hour are plotted in Fig. 4-6. These showd that the intensity increases and the FWHM decreases monotonically with increased the thickness of the PtMn layer. In general, these peaks of XRD became stronger and narrower as increasing the thickness and increasing the annealing time. Surprisingly, short time annealing also brought similar effect on phase transferred of PtMn. That was implied that short time annealing may have potential applied into the manufacturing process if high temperature process was needed. For the XRD peak of CoFe/NiFe fcc (111), after annealing, it also showed stronger intensity and narrower peak. This suggests the improvement of the crystal structure of the magnetic multi-layers after annealing.

The magnetization as a function of applied magnetic field (H) for samples with d = 15 nm and annealing at 275°C for 1 hour indicated as the inserted figure in Fig. 4-7 (a). In Fig. 4-7 (a) the curve with dots (●) shows data for sample annealing without external magnetic field (H_a); and the curve with squares (□) presents data for sample annealing under an applied field of 7,500 Oe. The hystersis loop near 4,300 Oe is manifested for curve with squares. This is related to the magnetic exchange effect between PtMn and SAF layers. The stronger coupling of SAF with PtMn would make the larger value for the H_{ex} in MTJ. Fig. 4-7 (b) shows the H_{ex} as a function of the thickness (d) of PtMn layer for samples annealed at 275°C for 1 hour within magnetic field of 7,500 Oe. H_{ex} is almost near zero for d $\leqq$ 8 nm, and it increases to 4,000 Oe for samples with d $\geqq$ 10 nm. Besides, our studies told us that if the field during annealing was not strong enough, the H_{ex} would not be induced or showed a smaller value. In the annealing cases with temperature higher than 400°C, the H_{ex} would not found even with annealing time as short as 10 minutes.

For investigating the practical usage of our samples in the MRAM system, the MR was

studied for samples after patterning. The MTJ sample with d = 15 nm, which had an ellipse shape with 2:1 ratio between long axis and short axis, showed near 30% MR ratio after annealing with 270°C for 5 hours at 8.5 kOe field as shown in Fig. 4-8 (a). Fig. 4-8 (b) shows the MR ratio of the sample in Fig. 4-8 (a) measured as a function of post-annealing time (T_{PA}). It is clear that 400°C is too high for our patterned samples. However, in the temperature range near 275°C, 10 minutes is the up-limit for our samples. By comparing the annealing processes of our samples with and without patterning, it shows clearly that the annealing temperatures can go up to 400°C to improve the structure of samples without patterning. However, annealing temperature of 275°C is too high for samples after patterning. The structure phase transformation temperature for PtMn is near 270°C, and, therefore, annealing process above 270°C for samples without patterning is necessary. For samples after patterning, the degradation of MR ratio might be come from the breakdown of the edges of the patterned samples as well as the complicated environments around the patterned samples.

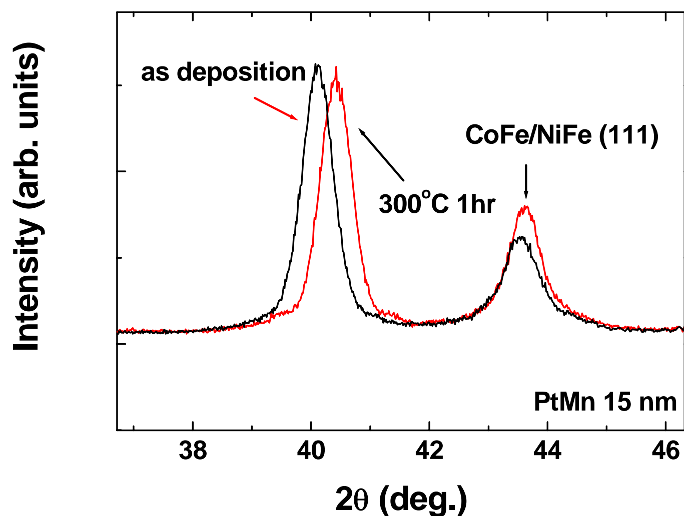

Fig. 4-1 The XRD patterns of the MTJ with 15 nm PtMn before and after annealing at 300°C for 1 hour.

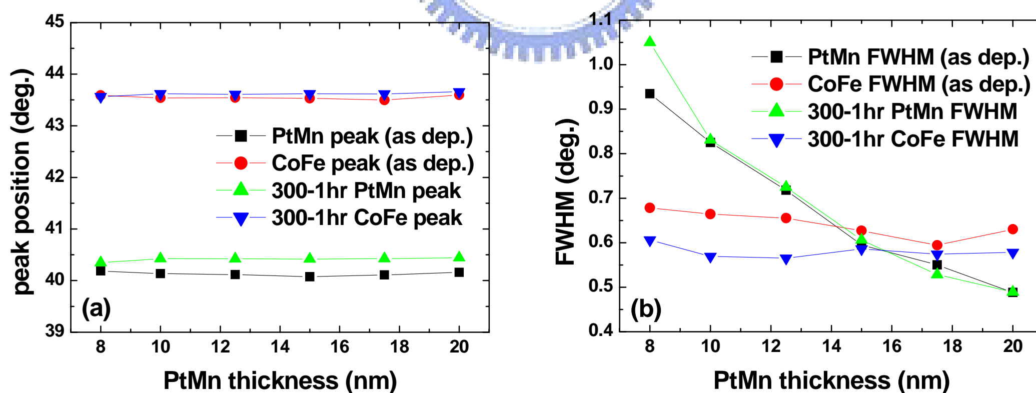

Fig. 4-2 The (a) peak-positions and the (b) FWHM of each peaks of PtMn and CoFe are functions of PtMn thickness and annealing treatment.

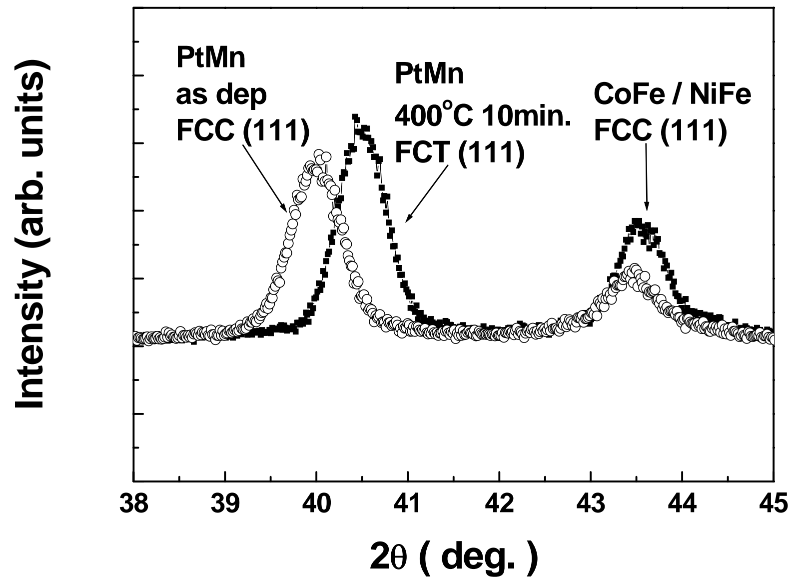

Fig. 4-3 The XRD intensity for PtMn, CoFe and NiFe as a function of diffraction angles for samples (with d = 15 nm) without annealing and annealing at 400°C for 10 minutes.

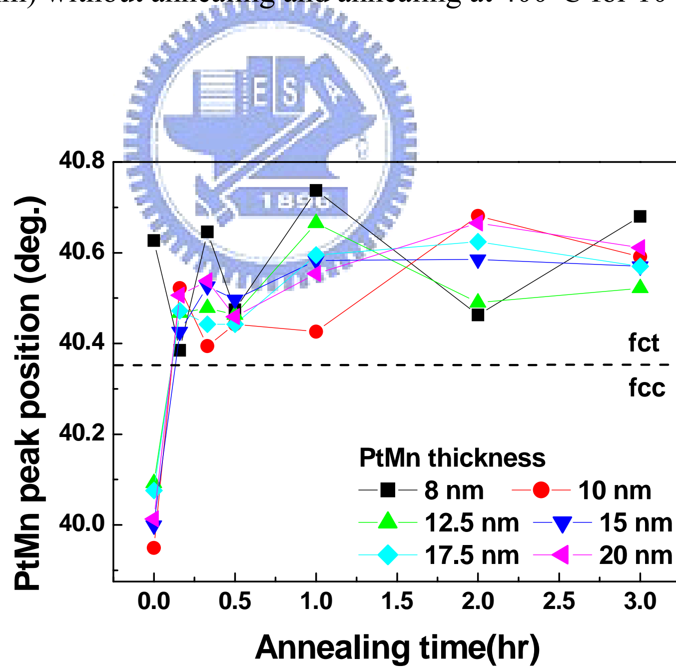

Fig. 4-4 The PtMn peak position of MTJ samples with different PtMn thickness after different 400°C annealing times.

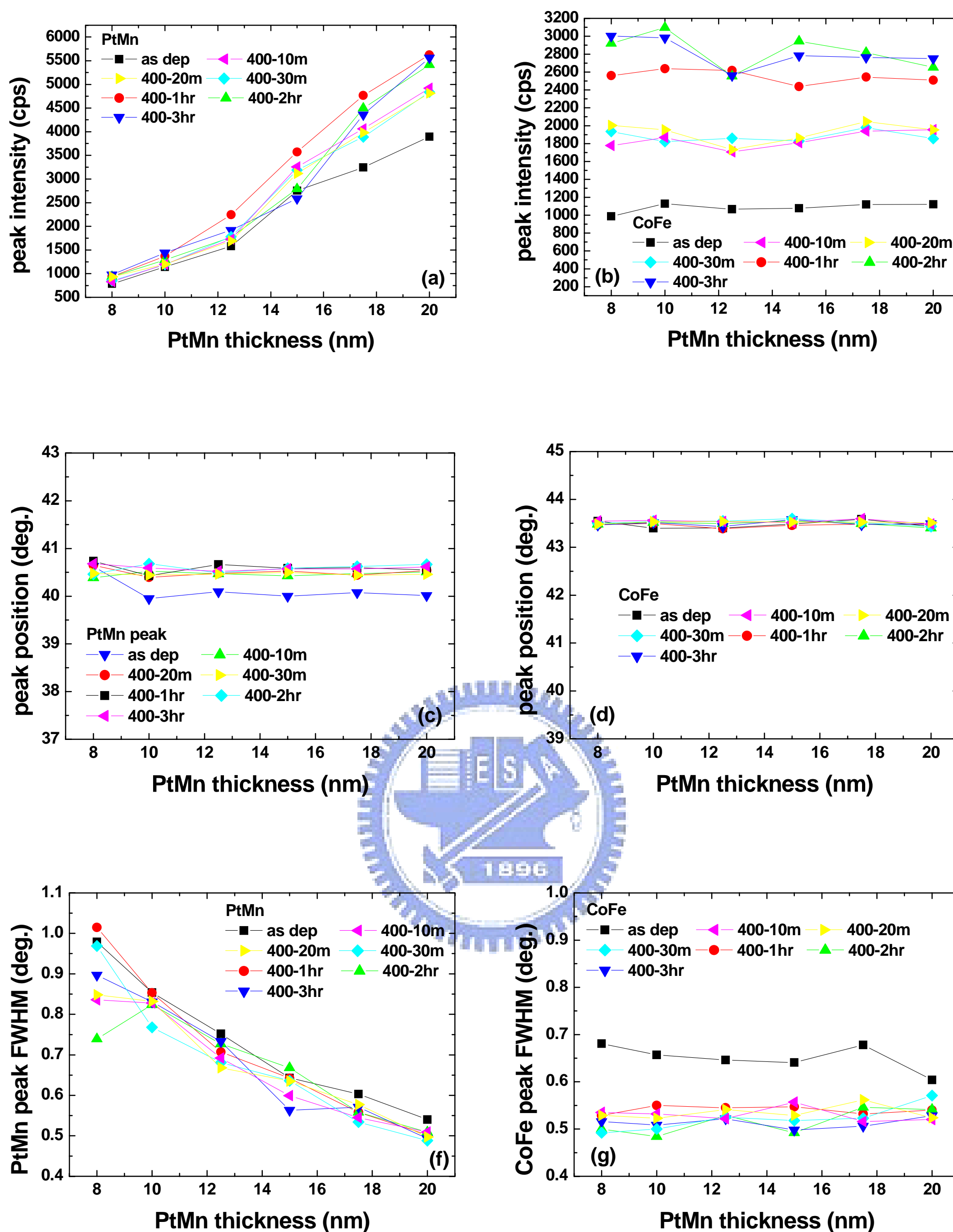

Fig. 4-5 The peak intensities ((a), (b)), the peak-positions ((c), (d)), and the FWHM of peaks of PtMn and CoFe ((f), (g)) for samples with d varied from 8 to 20 nm after 400°C annealing for different annealing time.

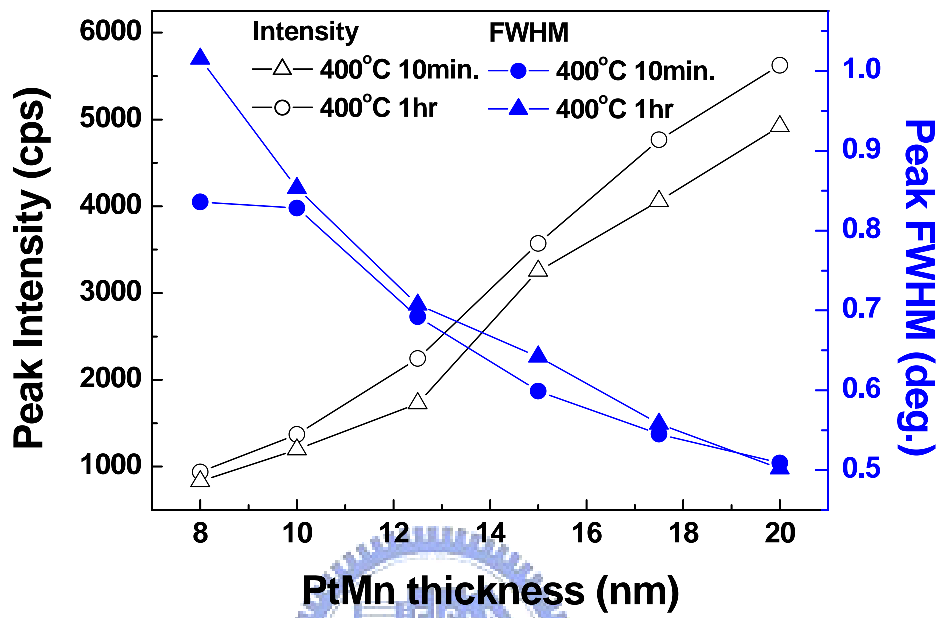

Fig. 4-6 XRD intensity and FWHM of PtMn peak for samples with d varied from 8 to 20 nm and annealing at 400°C for 10 minutes and 1 hour.

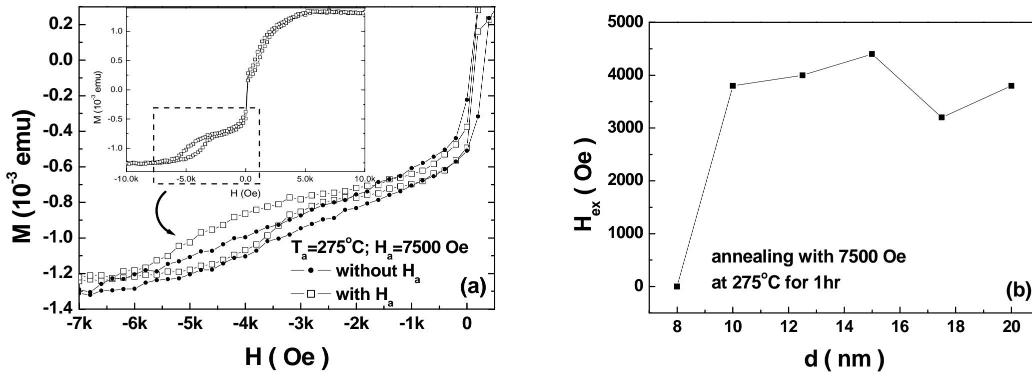

Fig. 4-7 (a) The PtMn base MTJ showed stronger H_{ex} after field annealing (□) (T_a = 275°C, H_a = 7,500 Oe) near 4,300 Oe instead of the weaker H_{ex} after annealing without field (●); (b) H_{ex} induced by PtMn was as a function of PtMn thickness (d).

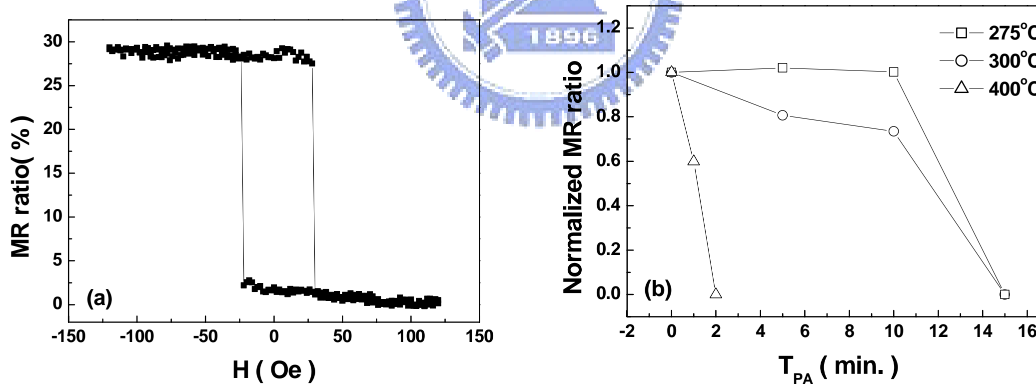

Fig. 4-8 (a) The MR loop of the PtMn based MTJ after patterning showed a MR ratio near 30 %; (b) Normalized MR ratio versus post-annealing time, T_{PA}, for different annealing temperature.

4-1-2 Os diffusion barrier in the CoFe/OsMn systems

Magnetic behavior is very sensitive to chemical composition, interface and structure, and therefore, interdiffusion due to heat treatment may cause problems. Many Mn-metal alloys used as the antiferromagnetic layer in magnetic devices have been extensively studied [112-114]; however, the Mn atom causes interdiffusion problems to degrading the overall performance [115-116]. In this section, the Os was found with potential to being good Mn atoms diffusion barrier. The thermal stability of a magnetic multilayer with insertion of an Os layer and how does the Os layer play its role on preventing Mn atoms from diffusing are discussed.

Two types of film structure were RF-magnetron sputtered on SiO_2/Si (100) substrate. One set of Ta/ CoFe/ Ru (Os) 0.8 nm/ CoFe/ PtMn was used to study the probability of replace the Ru in synthesis antiferromagnetic (SAF) film by Os. The other set of magnetic multilayers of protection layer/$Co_{90}Fe_{10}$/Os (d)/$Os_{20}Mn_{80}$ with an in-plane magnetic field of 200 Oe during the growth was used for investigating the diffusion barrier use of Os. The thickness of the CoFe and OsMn were fixed at 10 nm and 20 nm, respectively. The thickness of the Os layer, d, was varied from 0 to 2 nm. It is also important to prevent the specimen from oxidation during annealing with a capping layer. After the growth, these samples were ex-situ vacuum-annealed for 30 minutes at different temperatures (T_{an}) with a stronger applied field of 1 kOe along the easy axis.

As mentioned in section 1.1, the technology how to grow the antiferromagnetic OsMn film is protect by the US patent [11]. The OsMn film deposited in our system by using powder pressed OsMn target did not show antiferromagnetic properties. It was also apparent from the XRD analysis that our samples with $Os_{20}Mn_{80}$ layer do not show γ-phase and our sample's

properties do agree with Ref [12-13, 117]. However, the potential of Os to being diffusion barrier was found in the set of experiment trying to replace the Ru in the SAF structure by Os. Fig. 4-9 shows the MOKE measurements of CoFe/Ru (Os) 0.8/CoFe/PtMn ((a) and (b), respectively). The 0.8 nm Ru base SAF film was presented the typical SAF hysteresis loop after annealing at the 260°C at which the PtMn was phase changed from face center cubic (fcc) to face center tetragonal (fct). Only FM/AFM coupling between CoFe/PtMn was found in the case of Os base SAF type film indicated that the CoFe/Os 0.8 nm/CoFe/PtMn did not form SAF coupling. This result can be agreed to that the interlayer-coupling constant, J value, of Co/ Ru was nearly ten times larger to that of Co/ Os [118], and therefore, the magnetic properties did not be enhanced through using Os to replace the Ru layer in SAF structure. Nevertherless, the exchange field (H_c) of both films showed similar trend as the annealing temperature increasing, as shown in Fig. 4-10. The noticeable point is that the H_c of the Os base SAF type film was still appeared even after 400°C annealing while that of the Ru SAF film disappeared. The AES depth profile results used to analyze the diffusion phenomenon in both film structures are shown in Fig. 4-11. The Fig. 4-11 (a) and Fig. 4-11 (b) are presented the CoFe/Ru/CoFe/PtMn and CoFe/Os/CoFe/PtMn after 400°C annealing, respectively. The Co LM2 signal was almost continues in the Ru layer where Ru signal was vary weak. This indicated that the Ru layer was destroyed after heat treatment. On the other hand, the Co LM2 signal was slightly discontinues in the Os layer where Os signal was still exited, which meant the Os layer was stable after annealing. Furthermore, the Fe signals were not detected due to the signal overlapping between Co, Mn, and Fe. The Fe concentration in our used CoFe was only 10%, and the interdiffusion of Fe was less than Co [66]. The thermal degradation of such films did not result from Fe interdiffusion, thus the Fe signals can be ignored during mesurements. In adding to distinguish whether the nano oxide layer (NOL) resulting from the short exposing in air during sample preparing processes made the Os stabilized or not, another sample of CoFe/Ru/CoFe/PtMn, with thicker NOL between the Ru/ CoFe, was used to

analyze this issue. As seen from the fig. 4-11 (c), the annealed sample still disappear the Ru signal while the Co LM2 signal is more continues than that of Os base SAF type film. Even though the NOL was a kind of diffusion barrier [119], Os between two CoFe layers did show better thermal stability than Ru between two CoFe layers and indicated Os may have potential to be a diffusion barrier.

A 2 nm Os layer was added between CoFe and OsMn to study the diffusion barrier use. From the MOKE results, Os between CoFe and OsMn did not affect the coercivity field (H_c) at as-deposited state. The H_c changed slightly as increasing T_{an} until after 440°C annealing, as shown in Fig. 4-12 (a). Besides, the H_c of single CoFe layer was retained after 400°C annealing when Os interlayer was added. Compared with CoFe/OsMn without Os interlayer, the retaining of H_c was achieved even the d was as thin as 0.5 nm, as shown in Fig. 4-12 (b).

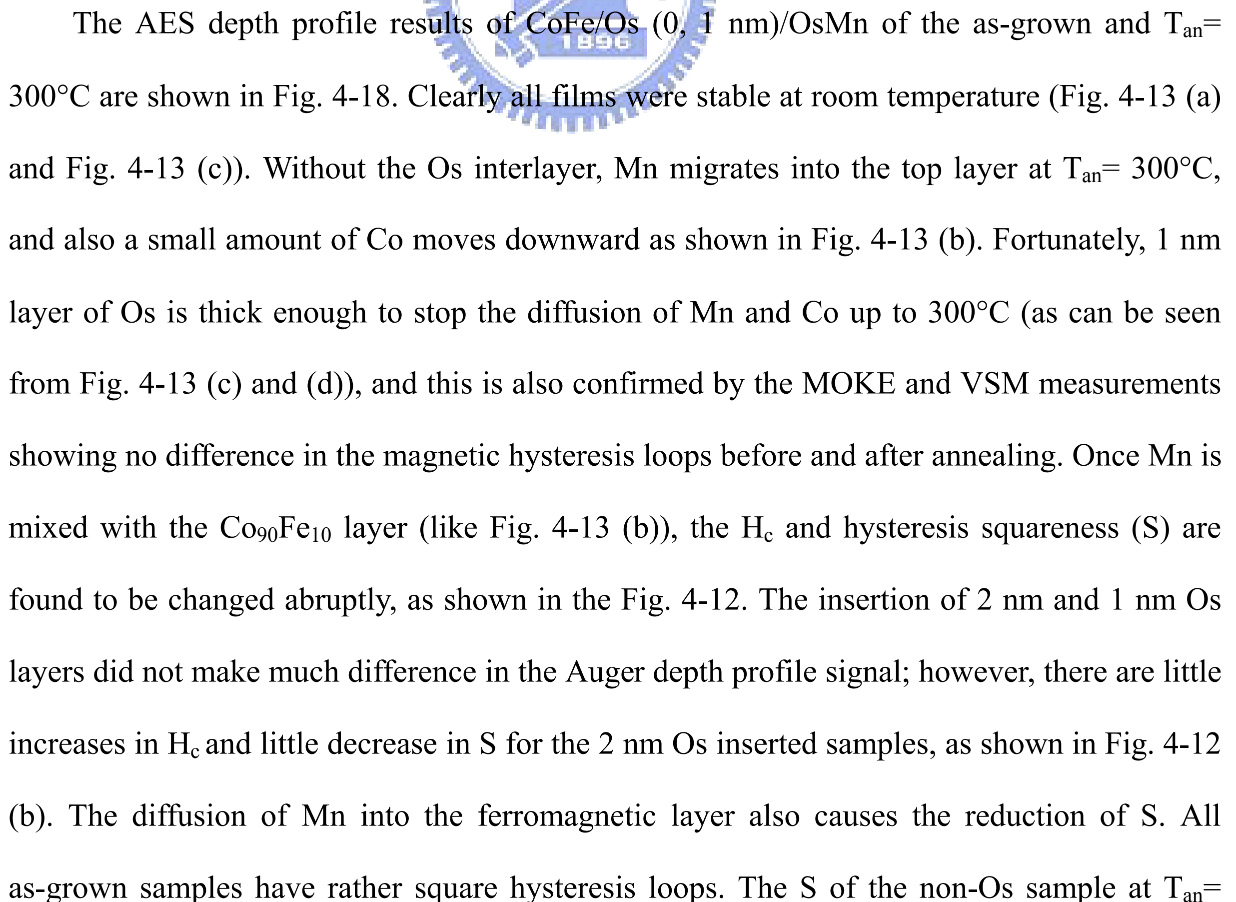

The AES depth profile results of CoFe/Os (0, 1 nm)/OsMn of the as-grown and T_{an}= 300°C are shown in Fig. 4-18. Clearly all films were stable at room temperature (Fig. 4-13 (a) and Fig. 4-13 (c)). Without the Os interlayer, Mn migrates into the top layer at T_{an}= 300°C, and also a small amount of Co moves downward as shown in Fig. 4-13 (b). Fortunately, 1 nm layer of Os is thick enough to stop the diffusion of Mn and Co up to 300°C (as can be seen from Fig. 4-13 (c) and (d)), and this is also confirmed by the MOKE and VSM measurements showing no difference in the magnetic hysteresis loops before and after annealing. Once Mn is mixed with the $Co_{90}Fe_{10}$ layer (like Fig. 4-13 (b)), the H_c and hysteresis squareness (S) are found to be changed abruptly, as shown in the Fig. 4-12. The insertion of 2 nm and 1 nm Os layers did not make much difference in the Auger depth profile signal; however, there are little increases in H_c and little decrease in S for the 2 nm Os inserted samples, as shown in Fig. 4-12 (b). The diffusion of Mn into the ferromagnetic layer also causes the reduction of S. All as-grown samples have rather square hysteresis loops. The S of the non-Os sample at T_{an}=

400°C is reduced to 0.25. Almost no interdiffusion evidence was found for samples with either 1 nm or 2 nm Os layers. S is slightly reduced from 0.96 at T_{an} = 400°C to 0.75 at T_{an}= 440°C. This could be due to our Auger system; the chemical information may be too small to detect. According to AES depth profile results of 400°C annealed samples, shown in Fig. 4-14, the insertion of 1 nm Os layer can also block the Mn diffusion channel and thus, retain the magnetic behavior.

As shown in Fig. 4-15, all samples showed S closed 1 and indicated the magnetization curve was very square at as-deposited state. After 400°C annealing, samples with Os barrier kept their S > 0.9 even though the Os thickness was as thin as
0.3 nm while S for non-Os sample was only 0.25 under the same process. Furthermore, the same behavior could be found on focusing the H_c varied as increasing Os barrier thickness. All samples showed a roughly the same H_c of 10 Oe at as-deposited. The H_c of annealed sample without Os changed from 9.5 Oe to 35 Oe (became near 4 times larger), while H_c for annealed samples with Os only slightly increased to 12.5 Oe (became 1.2 to 1.6 times larger than as-deposited for each thickness of Os). The Os interlayer thickness dependences of S and normalized H_c for 400°C annealed samples are summarized in Fig. 4-16. The normalized H_c, which was defined as $H_c\,(T_{an})$/ H_c (as-grown), was used to ignore the area difference between samples. The depth profile results and the improvements of Os on S and H_c of annealed CoFe layer indicated that a thin Os layer could prevent Mn atom from diffusion into the ferromagnetic layer after more than 300°C annealing. Because the inserting metal layer in the FM/AFM interface decreased the FM/AFM exchange coupling [120], the optimal Os barrier thickness which could not only retain the magnetic properties of the magnetic layer after annealing but also slightly decrease FM/AFM exchange coupling was an important factor to determine the barrier thickness. The 0.3 nm insertion Os layer could not only retain S of sample larger than 0.9 but also keep the H_c slightly increased to 1.6 times larger seemed to be

a suitable interlayer for FM/AFM magnetic film.

Since the improvement of Os layer on thermal properties was verified, a thin Os layer was added into the IrMn exchange coupled magnetic film to check the influence on the H_{ex}. Fig. 4-17 shows the VSM measurement for Ta/CoFe/IrMn/CoFe/SiO_2 (a) without and (b) with 0.3 nm Os interlayer respectively. The smaller H_{ex} was contributed from bottom CoFe seed layer, which was also exchange coupled by IrMn. In general, 350°C was too high for IrMn base magnetic multilayer because of it made high diffusion tendency of Mn atoms. The H_{ex} of as-deposited and 350°C annealed states were 100 and 190 Oe for sample with Os respectively. However, sample without Os barrier showed a H_{ex} of 55 Oe after 350°C annealing while that of as-deposited state was 105 Oe. These represented the Os stop the Mn atoms diffusion from IrMn to upper CoFe and made the H_{ex} increasing at such high temperature. On the other hand, the Os layer also seemed to decrease the tendency of Mn diffusing to the bottom CoFe layer because of the retaining of the H_{ex} contributed from bottom IrMn/CoFe was almost the same with as deposited state. The enthalpy of Mn in the Os and Co interface was -39 and -21 kJ/mole respectively (as shown in Table 4.1) [121]. It indicated that the Mn would be cohesive and stable when met the Os, thus had higher tendency to stay in Os/IrMn than in CoFe/IrMn interface. Compared with other material, Ta [68], having the same use, the enthalpy of Mn in the Os interface did show lower value (-32 and -14 kJ/mole for Os and Ta, respectively), thus brought out better thermal properties. It could be found from that the annealed sample with inserted Os layer made the whole magnetic behavior almost the same with the as deposited state. However, the sample without Os layer not only lost the exchange coupling of bottom IrMn/CoFe but also showed smaller exchange coupling of upper CoFe/IrMn. Furthermore, one of the possible diffusion models is exchange their own positions for neighbor two atoms, as shown in Fig. 4-18. The Os atom was too large for Mn atom to exchange their-own positions. These are also proved the Os has potential to be good

diffusion barrier.

Table 4.1 Calculated values of limiting partial enthalpies of solution and the heat of mixing for liquid binary manganese alloys (Data are from Ref. [121])

	$\Delta H^{mix}_{\{MnX\}}$ (kJ/mole)	$\Delta \overline{H}^{\circ\ interface}_{Mn\ in\ X}$ (kJ/mole)
Os	-9	-32
Co	+2	-21
Fe	0	+1
Ta	-4	-14

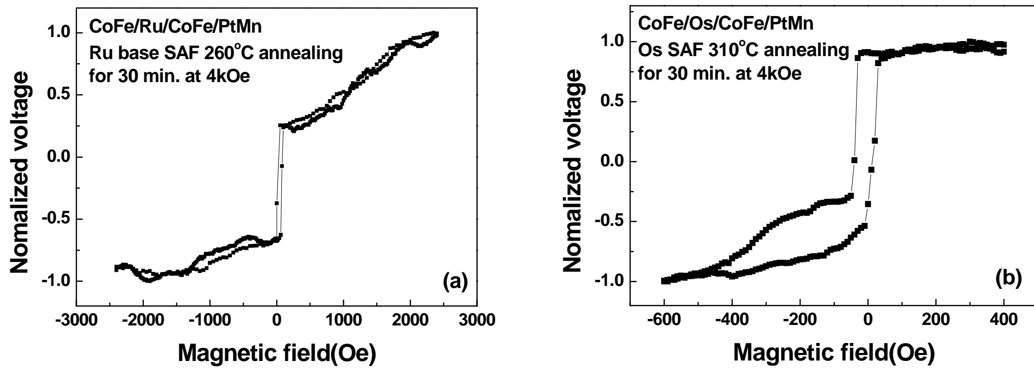

Fig. 4-9 The 400°C annealed MOKE measurements of (a) CoFe/Ru 0.8/CoFe/PtMn and (b) CoFe/Os 0.8/CoFe/PtMn, respectively.

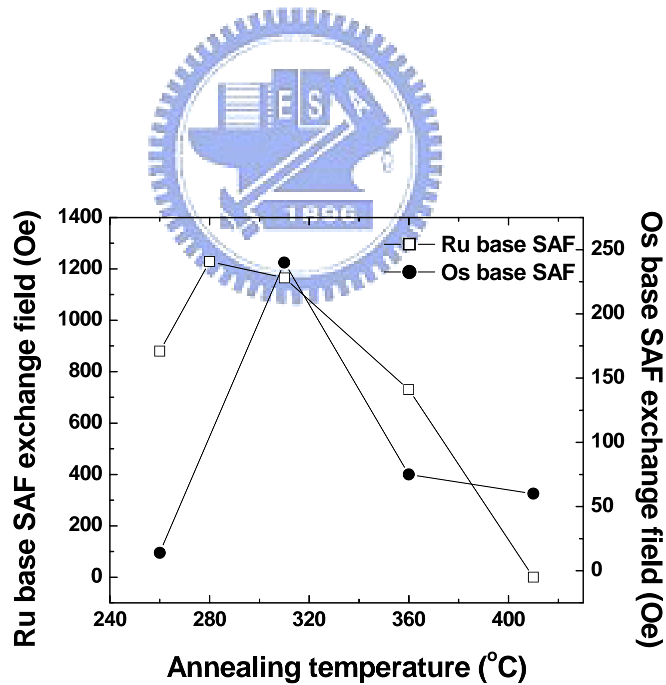

Fig. 4-10 The H_{ex} of Ru and Os base SAF film are as functions of the annealing temperature.

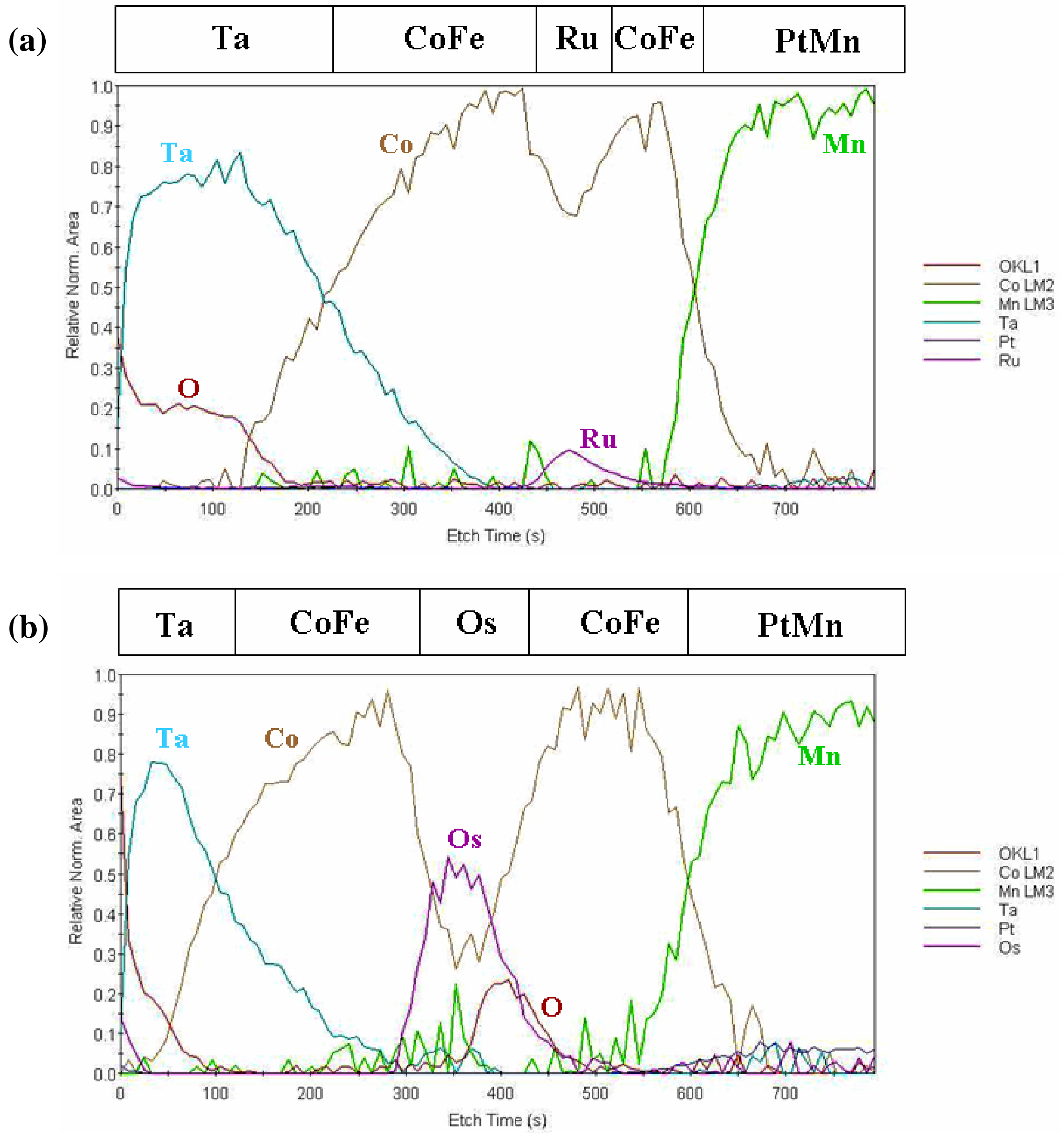

Fig. 4-11 The AES depth profiles of (a) Ru base SAF, and (b) Os base SAF after 400°C annealing.

(c)

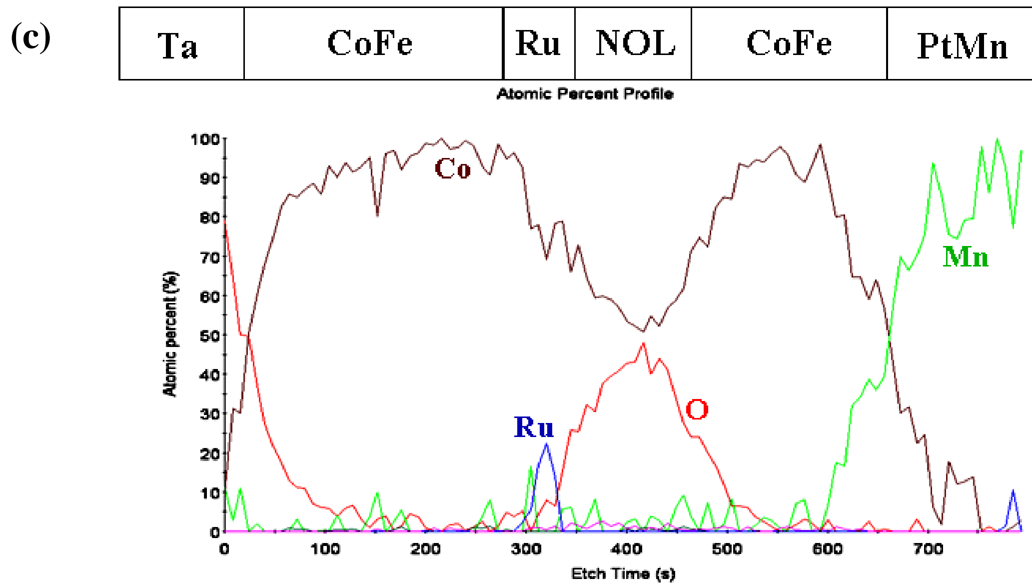

Fig. 4-11 (continued) The AES depth profiles of (c) Ru base SAF with thick NOL after 400°C annealing.

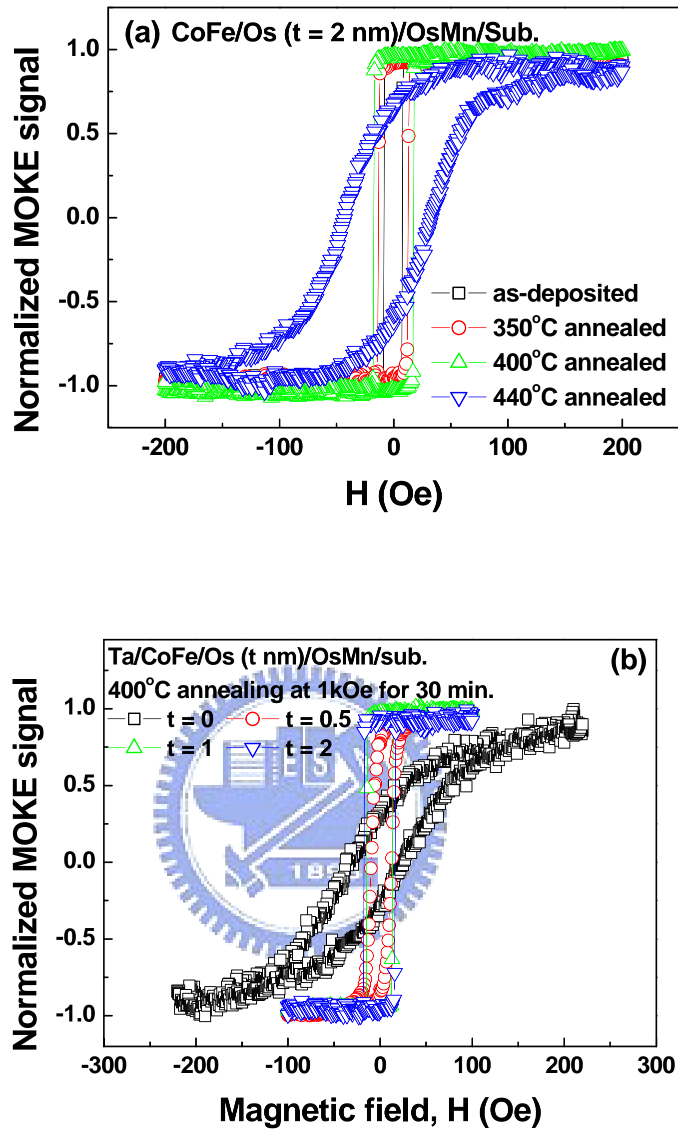

Fig. 4-12 The MOKE measurements of CoFe/Os (d)/OsMn. (a) shows that 2 nm Os can be retained the CoFe hysteresis loop as the same with as-deposited even after 400°C annealing. (b) indicates that the CoFe hysteresis loop can be retained can be retained after 400°C annealing even the inserted Os layer was as thin as 0.5 nm.

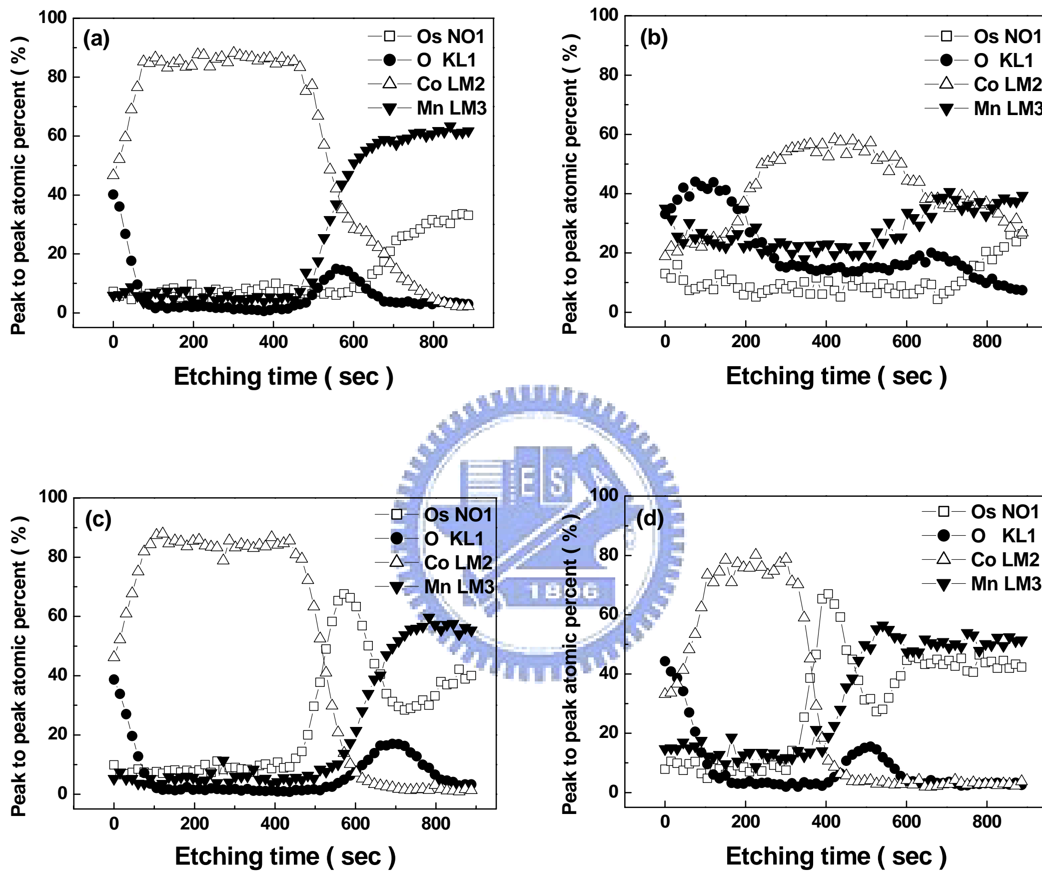

Fig. 4-13 AES-depth profiles for the CoFe/Os (d nm)/OsMn multilayer before (a), (c) and after (b), (d) annealed at 300°C ((a), (b): d=0; (c), (d): d=1).

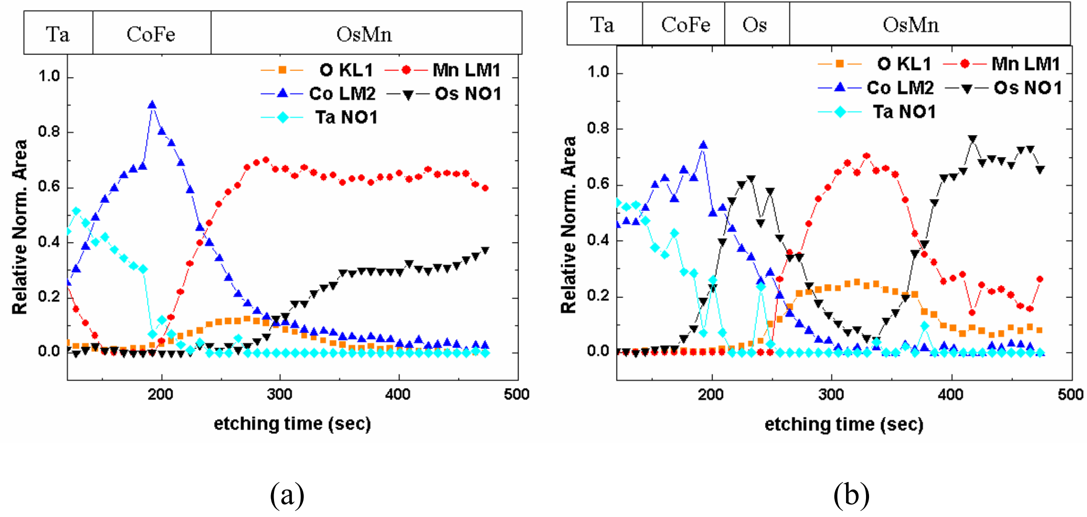

(a) (b)

Fig. 4-14 The AES depth profiles of Ta/CoFe/OsMn (a) without and (b) with 1 nm Os interlayer as a diffusion barrier after 400°C annealing.

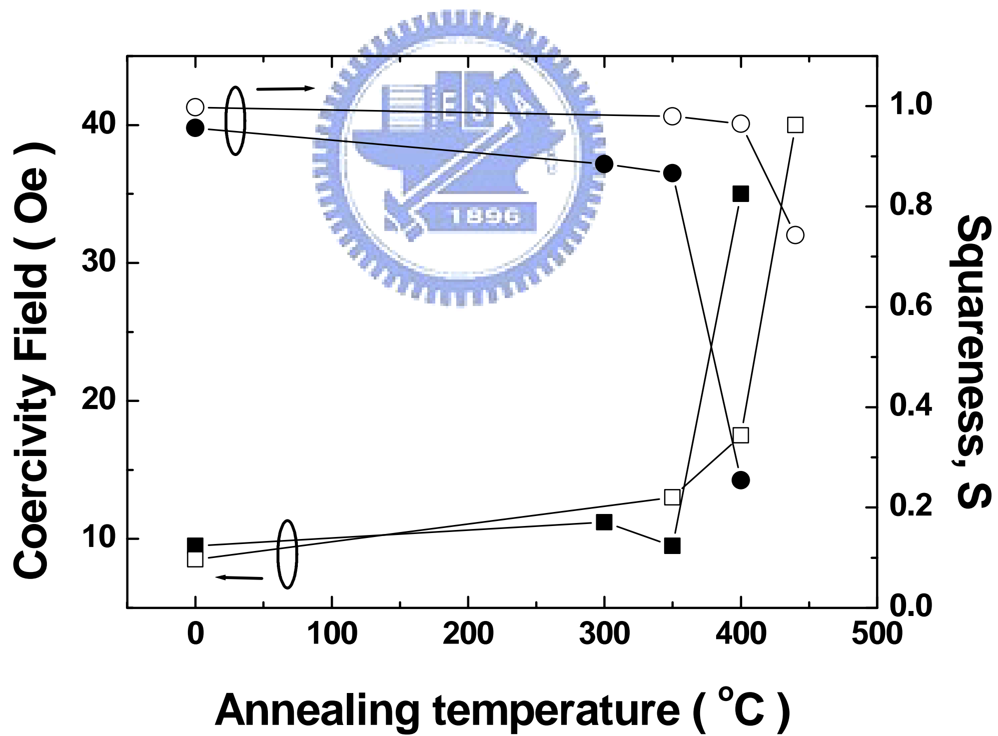

Fig. 4-15 The temperature dependence of H_C (■ and □) and S (● and ○) in the CoFe/Os (d nm)/OsMn multilayer, which indicated by d = 0 (dark symbol) and d = 2 (open symbol). The annealing conditions are 30 minutes at 1 kOe external field.

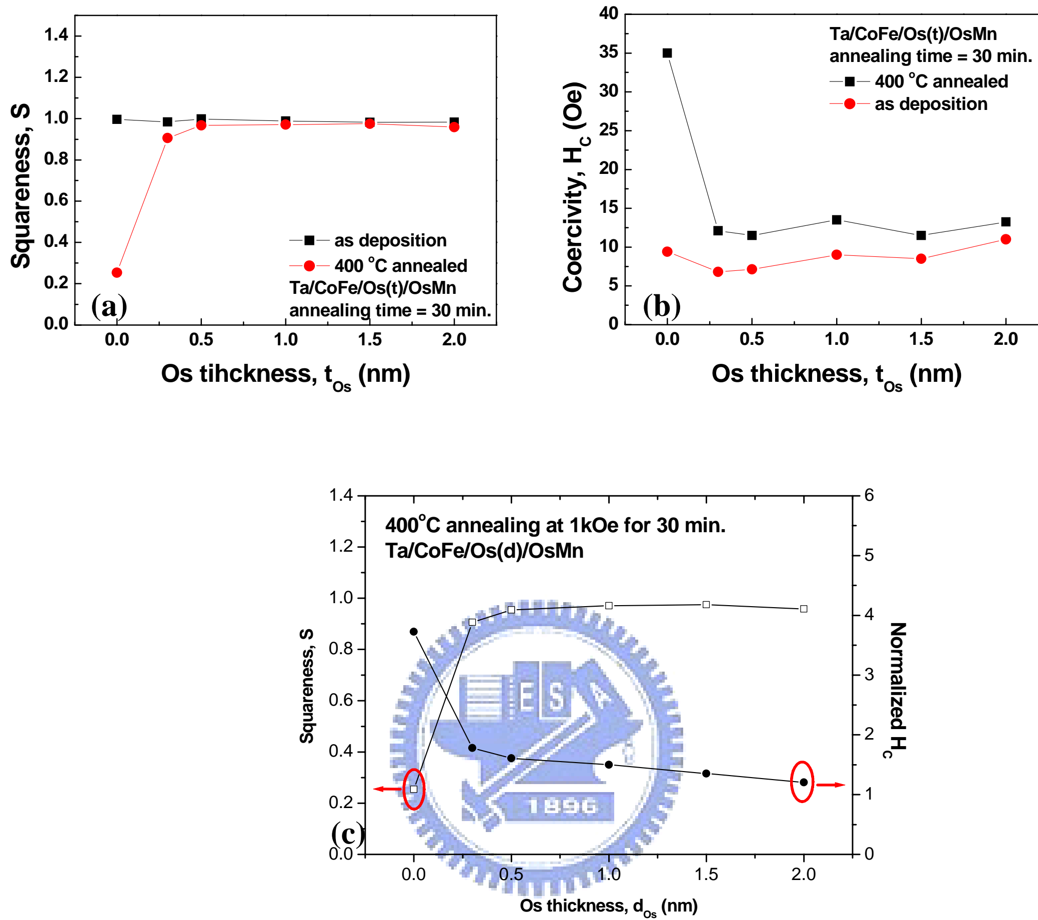

Fig. 4-16 The Os barrier thickness dependence of: (a) the magnetization curve squareness and (b) the coercivity field in the Ta/CoFe/Os (d nm)/MnOs before and after 400°C annealing. (c) is the Os interlayer thickness dependence of the squareness and the normalized H_c after 400°C annealing.

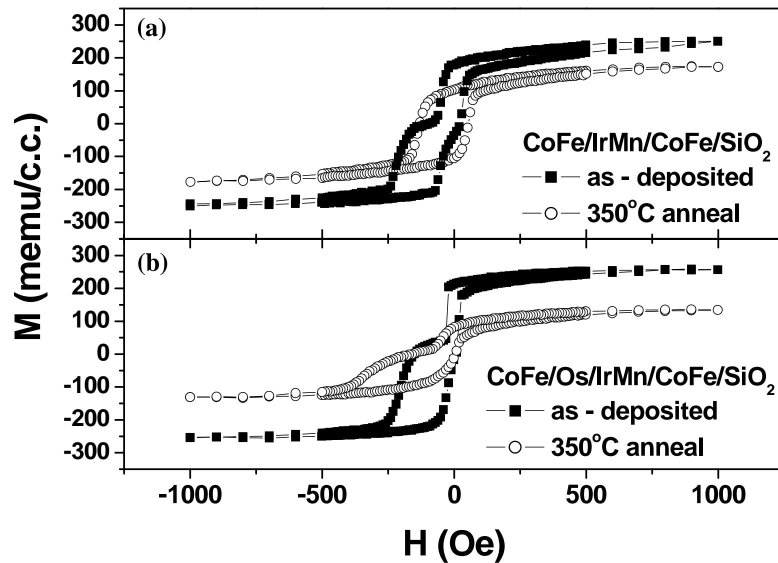

Fig. 4-17 The VSM measurement of the Ta/CoFe/IrMn/CoFe/SiO_2 multilayer (a) without and (b) with a 0.3 nm Os barrier inserted in the upper part of the CoFe/IrMn interface. The H_{ex} of the annealed sample with the 0.3 nm Os barrier (○) was larger than that of the as-deposited state (■).

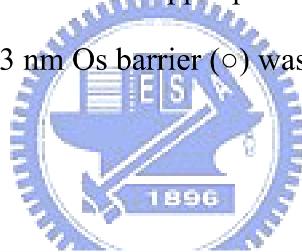

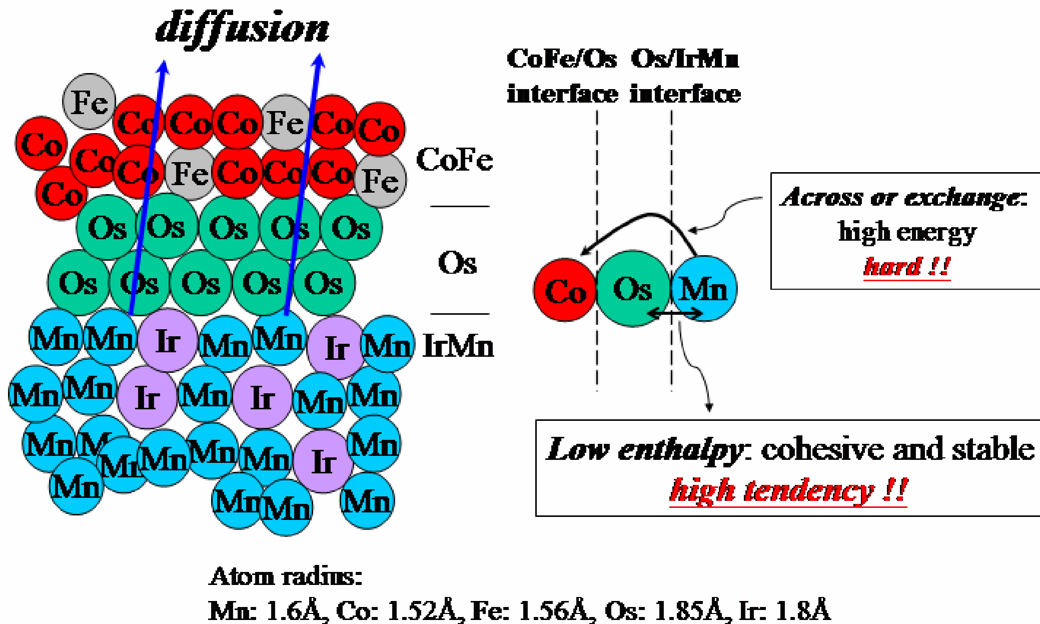

Fig. 4-18 An illustration of the possible diffusion model of Mn atoms interdiffusion in the CoFe/IrMn interface.

4-2 Buffer layer use and growth of Os (0002)

4-2-1 Buffer layer use of Os in CoFe/IrMn systems

The magnetic layers are the essential ingredients of spintronics, whose properties, such as structure, thermal stability, and magnetization, have large influences on the overall performances in spin devices. A suitable buffer layer is needed for an antiferromagnetic (AFM) layer to induce the ferromagnetic/antiferromagnetic (FM/AFM) coupling in magnetic tunnel junction (MTJ) or spin valve (SV) structures [122]. The control of the crystallinity of memory cells is a new issue worth study since a crystal MTJ structure results in higher MR ratios [8]. Many face center cubic (fcc) metals, such as NiFe and NiFeCr, are used to provide strong fcc (111) orientation in magnetic films [123]. The previous report is described that the hexagonal closed packed (hcp) structure buffer layers, such as Ti, Hf, and Zr, could enhance the face center cubic (fcc) (111) structure of the IrMn to induced exchange field (H_{ex}) on Si substrates [124]. Furthermore, the hcp structure Ru buffer layers could also enhance the exchange field (H_{ex}) of Mn_3Ir/Co-Fe and avoiding interdiffusion during growth [125] due to its high melting point. However, there are no papers reported the growth of IrMn with the hcp structure Osmium (Os) buffer layer, and the uses of the Os are also rare. In this section, we investigate the characterizations of the Os being a buffer layer grown on different substrates.

Three types of substrates were used to examine the characterizations of the Os being a buffer layer to grow the magnetic films as the following two series. The first series of Ta/CoFe (10nm)/IrMn (15nm)/Os (t_{Os})/Ta/SiO_2 with thickness of Os buffer was prepared by magnetron sputtering with varying t_{Os} from 1 to 11 nm, where the Ta on the SiO_2 was to form the atomic surface to improving the Os adhesion. The focus of this series was finding out the proper conditions for CoFe to be exchange coupled by IrMn in the as deposited state. The

other textured structure series of Ta/CoFe 10/IrMn 30/Os (t_b)/Cu 30/Si (100 or 111) was also grown by magnetron sputtering, where the thickness was shown in nm. The Os layer acted as a buffer layer for IrMn growth and varied from 0 to 30 nm. Before depositions, Si wafers were first cleaned with acetone to degrease them and dipped into 10 % HF solution for several seconds to form a hydrogen-terminated surface. Then they were loaded into the vacuum chamber immediately. According to the metal-metal epitaxy on silicon (MMES) method [100, 125], the Cu (002) epitaxy seed layer was grown on the Si (100) wafer first, and the Os film was sequentially deposited at about a 5 mTorr pressure of pure Ar gas without breaking the vacuum. No external heating was applied to the substrates during films growth. As described in the previous section, the Os showed potential to be a diffusion barrier in magnetic films. Thus, the thermal stability of the textured structure magnetic film will also be discussed in this section. A thin Os diffusion barrier was inserted in the interface of CoFe/IrMn on the cleaned H-Si (100). The textured and poly-crystalline samples were denoted as the CoFe/IrMn with and without the Os buffer layer, respectively, while the Os diffusion barrier with variation thickness, d, varied from 0 to 1 nm. After deposition, all samples were subjected to magnetic field annealing at 3 kOe and at different temperatures ranged from 150°C to 400°C for 30 min.

Os, like Ru and Zr, is hcp structure, and the IrMn (111) texture enhancement was found in the bottom series from the XRD analysis, as shown in Fig. 4-19 (a). The 50 nm Ta layer did not result in IrMn (111) and CoFe (111) texture, and only a broaden and weak peak of Ta (110) could be found by the XRD measurement. However, the buffer layer consisted of Os 11nm/ Ta 5 nm enhanced the IrMn (111) and CoFe (111) texture can be found clearly. The IrMn (111) and Os (0002) diffraction peaks were hard to distinguish becaused they had roughly the same spacing distance. Fig. 4-19 (b) shows the IrMn (111)/Os (0002) and CoFe (111) diffraction peaks could be clearly found when the thickness of the Os was greater than 5 nm. In addotion,

MOKE analysis showed that the exchange coupling was produced even when the Os buffer was as thin as 1 nm, as shown in Fig. 4-20. A 120 Oe of H_{ex} was achieved by using an 11 nm of Os as a buffer layer. Although the IrMn (111)/Os (0002) and CoFe (111) peak intensities were weak in the thinner Os inserted samples, the H_{ex} was still produced after deposition. With increases in the thickness of the Os buffer, these diffraction peak intensities became increasingly clear. The H_{ex} and diffraction peak intensities of IrMn (111)/Os (0002) and CoFe (111) are proportional to the thickness of the Os. This means that the Os buffer not only enhances the IrMn (111) and CoFe (111) texture but also results in a clear H_{ex} in magnetic films.

The XRD results of Os/Cu/Si (100) and Cu/Os/Cu/Si (100) are presented in Fig. 4-21 (a). Obviously, a Cu (002) peak (near 51°) and an Os (0002) peak (near 41.78°) appeared when Os/Cu was put directly on Si (100). Since Os is an hcp metal and the (0002) surface, the basal plane of the hcp structure, has the same atomic arrangement as that of the fcc (111) plane. Thus, other fcc metals growing on top of the Os (0002) plane would grow to form the fcc (111) plane with small enough lattice mismatch. Evidence of this relationship was obtained by putting another Cu layer on the Os, and the clear Cu (111) peak overlapping with the Os ($10\underline{1}1$) peak near 43.5° was observed. However, as shown in Fig. 4-21 (b), the Cu on H-Si (111) neither forms obvious Cu (111) nor Cu (002) with such a thin Cu layer. The CoFe/IrMn on Os/Cu/Si (100) showed a strong peak near 41.5°, including of the Os (0002) and the IrMn (111) ($2\theta = 41.57°$). A small CoFe (111) peak ($2\theta = 44.2°$) was also overlapped with the Os ($10\underline{1}1$) peak. By contrast, the IrMn grown on Cu/Si (100) only showed the IrMn (002) ($2\theta = 47.8°$) instead of IrMn (111) due to the lower lattice mismatch between IrMn and Os. The lattice constants of Cu, Os, IrMn, and CoFe were 3.615, 2.73, 3.76, and 3.547 Å, respectively. Thus, along the epitaxial growth direction (fcc [111] of IrMn, CoFe, and hcp [0002] of Os), the relative distances between two neighboring atoms were 2.556 Å (the [110] direction of the

Cu (002) grown on H-Si (100)), 2.73 Å (Os), 2.658 Å (IrMn), and 2.508 Å (CoFe), respectively. The mismatches between each layer were 6.8% (Cu (002)/Os (0002)), -2.64% (Os (0002)/ IrMn (111)), and -5.64% (IrMn (111)/ CoFe (111)), respectively. All the mismatches were smaller than 7%, below which metal film can be epitaxially grown. Since the lattice mismatches between each layer were sufficiently small, the fcc CoFe/IrMn growing on top of the Os (0002) plane could form the fcc (111) orientation, obtaining higher H_{ex} [124]. That is the main reason to control the film structure. Compared with Os, other hcp materials, such Ti (a=2.95 Å), Hf (a=3.196 Å), and Zr (a=3.232 Å), showed relatively high lattice mismatches in the interface: -9.9% (Ti), -15.99% (Hf), and -17.76% (Zr), respectively. Therefore, the Os does show lower lattice mismatching and is suitable for epitaxial growth of magnetic films. However, the CoFe/IrMn only showed a very weak IrMn (111) peak on Os/Cu/Si (111), while essentially no peaks appeared when films were grown on Cu/Si (111). No Cu (002) formed on H-Si (111) when the Cu thickness was only 30 nm; thus, the lattice mismatch calculation mentioned above was non-tenable in this case. Interestingly, on the Os/Cu/Si (100), the intensity of the Os $(10\bar{1}1)$ peak was stronger than that of the Os (0002) peak when t_b was thinner. The intensity of the Os (0002) peak rose more sharply than that of the Os $(10\bar{1}1)$ peak as t_b increased, which indicated that the crystalline structure of the Os was changed. Thus, the surface states may be more suitable for IrMn (200) surface growth in the initial growth state of Os growth. At these conditions, the IrMn (200) peak was stronger than the IrMn (111) peak. That the CoFe film on IrMn/Os/Cu did not show an obvious (111) peak may be attributed to the low intensity due to its lower thickness.

As seen from Fig. 4-22, the intensity of the IrMn (111) ($I_{IrMn\,(111)}$) on both substrates was a function of the t_b. Only a weak IrMn (111) peak could be found when the t_b were larger than 20 nm. This indicated that the film was weakly-oriented in the normal direction. The IrMn (200) peak appeared on H-Si (100) when the t_b were not thick enough, and the $I_{IrMn\,(111)}$ on

H-Si (100) increased as the t_b increased. This indicates that the growth of IrMn film can be controlled. The increment of the $I_{IrMn\,(111)}$ as t_b increased was sharper, while the $I_{IrMn\,(200)}$ was kept constant. The relative peak intensity on H-Si (100), defined as $I_{IrMn\,(111)}$ / $I_{IrMn\,(002)}$, is also shown in Fig. 4-22. The $I_{IrMn\,(111)}$ and $I_{IrMn\,(200)}$ were nearly the same when t_b were less than 10 nm, and then the $I_{IrMn\,(111)}$ was raised sharply. According to these results, the increasing t_b restrained the growth of the IrMn (200) and made the surface change to a suitable surface mesh on H-Si (100) for IrMn (111) growth. Thus, Os plays an important role in IrMn structure tuning.

As revealed in Fig. 4-22, $I_{IrMn\,(111)}$ on both H-Si (100) and H-Si (111) had roughly the same intensity when t_b was thinner, while both of the two cases showed roughly similar magnetic properties. However, the hysteresis loops of both cases showed different squareness (S), which is defined as Mr/Ms, and implied different magnetization reversal processes. As the t_b increased, IrMn (111) structure became much better on H-Si (100), thus, making the better CoFe (111) structure and the magnetization switching of CoFe was more coherent, showing from that the S was very approaching to 1, than that on H-Si (111). Fig. 4-23 (a) shows the M-H loop of CoFe/IrMn/Os 30/Cu on H-Si (100) and H-Si (111), respectively. The non-square hysteresis loop of the CoFe on H-Si (111) indicated that the number of domains is larger than that of the square one due to the more disorder magnetic moments aligning, thus needing more domain nucleations and domain-wall motions to reverse the whole magnetization. On the other hand, a roughly 180 Oe of H_{ex} of CoFe/IrMn was obtained on both H-Si (100) and H-Si (111) with the 30 nm Os buffer layer, while the $I_{IrMn\,(111)}$ showed very different values on both substrates. One of the factors affecting the initial value of H_{ex} may come from the external field during film growing. An annealing treatment was performed as a training effect to eliminate this probable factor. Fig. 4-23 (b) shows these two M-H loops after 200°C annealing. It is clearly found that the H_{ex} on H-Si (100) ($H_{ex\,(100)}$) and

H-Si (111) ($H_{ex\,(111)}$) were 370 and 310 Oe, respectively. A 60 Oe increment of the H_{ex} on H-Si(100) indicates that the larger H_{ex} came from the better crystalline structure. Certainly, annealing improves the crystallinity of both samples. However, the initial state also determined the degree of improvement in the crystalline structure because the superior crystalline sample may have grain growth occurring first, without grain nucleation processes. On the other hand, the superior crystalline structure sample at the as-deposited state would have much better crystallinity than the inferior one. Thus, the interface of the CoFe/IrMn on H-Si (100) is conformed more closely to the ideal interface model, as stated by Meiklejohn and Bean [40], than that on H-Si (111). According to the assumptions of the model, the magnetic moments were aligned more parallel, thus giving a larger H_{ex}. That is strong evidence of the improvement of the film structure due to using an Os buffer layer.

The H_{ex} as a function of annealing temperature (T_a) for the textured and the poly-crystalline samples are shown in Fig. 4-24. The IrMn (111) and Os (0002) peaks were not shown in the XRD pattern of the poly-crystalline samples, while the textured samples were shown good crystalline structures, as revealed in Fig. 4-21 (a). The H_{ex} of the textured samples (~ 200 Oe) is larger than that of the poly-crystalline samples (~ 180 Oe) at as-deposited. The Os seed layer provided a very suitable surface mesh; therefore the magnetic films grown with very high textured fcc (111) crystallinity showed more coherent magnetic moments alignment. According to the ideal interface model [40], these high textured samples have more ideally interfaces. The regular magnetic moments alignment made the θ_F (the angle between magnetization of FM and easy axis) near zero and brought the highest exchange anisotropy energy ($K_e\cos\theta_F$, K_e: the interfacial coupling constant). Thus, the textured samples showed a larger H_{ex} than the poly-crystalline ones. It is clearly found that the poly-crystalline samples obtain maximum H_{ex} ($H_{ex,\,max}$) at 200°C and H_{ex} disappeared abruptly when T_a was higher than 250°C. However, the textured ones obtained $H_{ex,\,max}$ at 250°C and H_{ex} was lost

gradually as T_a increased. The H_{ex} of the textured samples vanished at 350°C while roughly no H_{ex} appeared for the poly-crystalline samples after the 275°C annealing. By using Os/Cu buffer layer, the improvements on temperature, at which the $H_{ex,max}$ appeared and the H_{ex} disappeared, are 50°C and 75°C respectively. Some studies point out that the diffusion of Mn atoms into the ferromagnetic layer reduced the H_{ex} [112]. In these two types of samples, the poly-crystalline samples could be seen as with a crystal-matrix with more grain boundaries coming from its random surface atomic arrangement while the textured ones exhibited fewer grain boundaries due to its much better crystallinity. The loose atomic arrangement made the occurrence of diffusion appeared easily. Since atoms diffuse much more rapidly along the grain boundaries than through the bulk and atom diffusion fluxes decrease grain size increase [127]. Then, more grain boundaries provided more diffusion paths [128] for Mn atoms to diffuse in to the CoFe layer. When samples were annealed at high temperatures, the diffusion at the grain boundaries occurred more easily. Thus, the textured samples showed better thermal stability after high temperature annealing. As shown in Fig. 4-25, the IrMn film structure does not change obviously as T_a increased. The clear destruction of film structure was appeared after 400°C annealing. However, the temperature dependence of H_{ex} showed that the reduction of H_{ex} was appeared after 200 or 250°C annealing, and the film structure can still keep under such conditions. Thus, the reduction of H_{ex} could be less dependent on structure destruction.

Furthermore, a thin additional Os barrier between the CoFe and IrMn layers also improved the thermal stability. From the XRD data (as shown from Fig. 4-26), no obvious changes were found, and hence it indicated that the insertion of the Os barrier did not affect the crystalline properties. The $H_{ex,\,max}$ of textured sample with d = 0.3 nm also appeared at 250°C, as shown in Fig. 4-27. However, it decreased slowly than that of the textured sample with d = 0 nm as temperature rising, and finally the H_{ex} vanished at 400°C. The 0.3 nm Os

inserted textured CoFe/IrMn film showed the 50 ℃ improvements on the temperature at which the H_{ex} disappearing. Interestingly, the textured samples with d = 1.0 nm also showed the $H_{ex, max}$ of 15 Oe at 250°C (as shown in Fig. 4-28), and the H_{ex} of those still existed after 400°C annealing. This finding was agreed with the study by Thomas et al [120] that the interlayer between the FM/AFM layers reduces the exchange coupling. The bell-shape curves appeared in the temperature dependence on the H_{ex} for the textured samples with each d. The H_{ex} dependence on the Os barrier thickness is shown in Figure 4-29. Without the Os diffusion barrier, the H_{ex} was decreased immediately from 240 Oe in the as-deposited state to 50 Oe after 300°C annealing; however, with d > 0, all 300°C annealed samples, show larger H_{ex} than that of the as-deposited state. The H_{ex} decreased as d increasing. Furthermore, the H_{ex} of the samples with d = 0.1 nm increased the H_{ex} from 170 Oe to 180 Oe after 300°C annealing. Blocking of the diffusions of Mn atoms by Os layer is previously investigated in the section 4-1-2, and the results of this study also indicated the similar phenomenon. The thicker d caused a greater rise of the H_{ex} after annealing because fewer Mn atoms entered into the CoFe layer. In comparison, there was no barrier to stop the Mn atom diffusion in the sample without the Os barrier; thus, the exchange coupling was reduced, leading to a small H_{ex}. The VSM measurement of sample with d = 0.1 nm is shown in Fig. 4-30. It clearly shows that the hysteresis loop was not changed very much, and a thermal reduction of half of the magnetic moments and a slight increment in H_{ex} (170 Oe at as-deposited state and 180 Oe after annealing, respectively) were found. It indicated that the magnetic properties were also retained after 300°C annealing even though the Os barrier as thin as 0.1 nm. In a comparison with the sample without the Os barrier, the retention of the H_{ex} of sample with d = 0.1 nm was very obvious.

Base on the results of this section, Os really showed good buffer layer properties for growing the magnetic films. As mentioned in the section 4-1-2, Os also showed good

diffusion barrier properties in magnetic films. Such superior characteristics will suggest that Os metal has the potentials to be the material with two uses in magnetic film structure. The unit material, Os, as diffusion and buffer layers would make the deposition system with limited source could get effective and efficiency use.

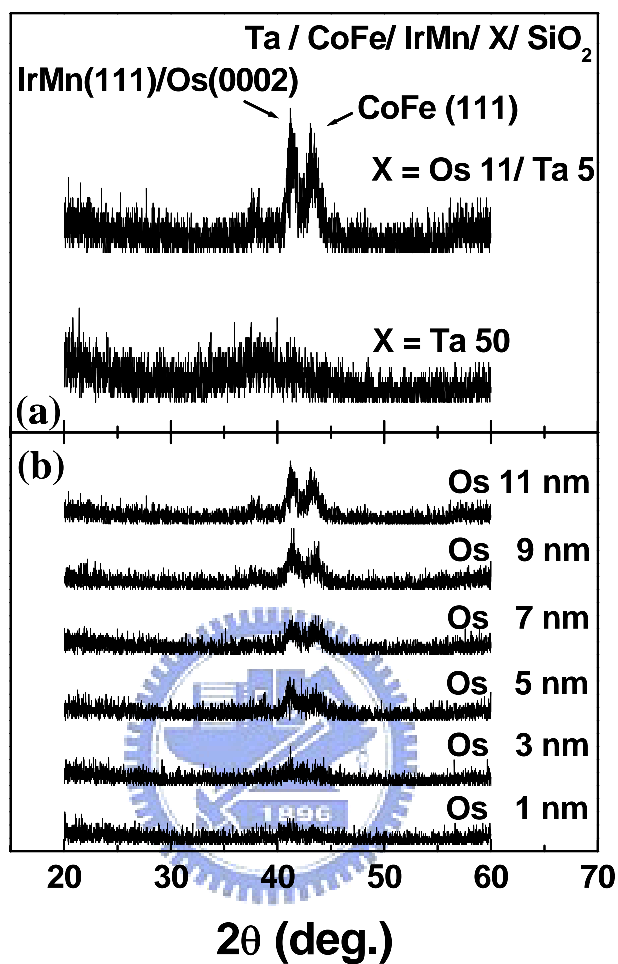

Fig. 4-19 The XRD measurements of the Ta/CoFe/IrMn/Os/Ta/SiO_2 multilayer: (a) the influence of the IrMn exchange coupled CoFe films with and without the Os buffer and (b) enhancement of the diffraction peaks varied as increasing of the Os thickness.

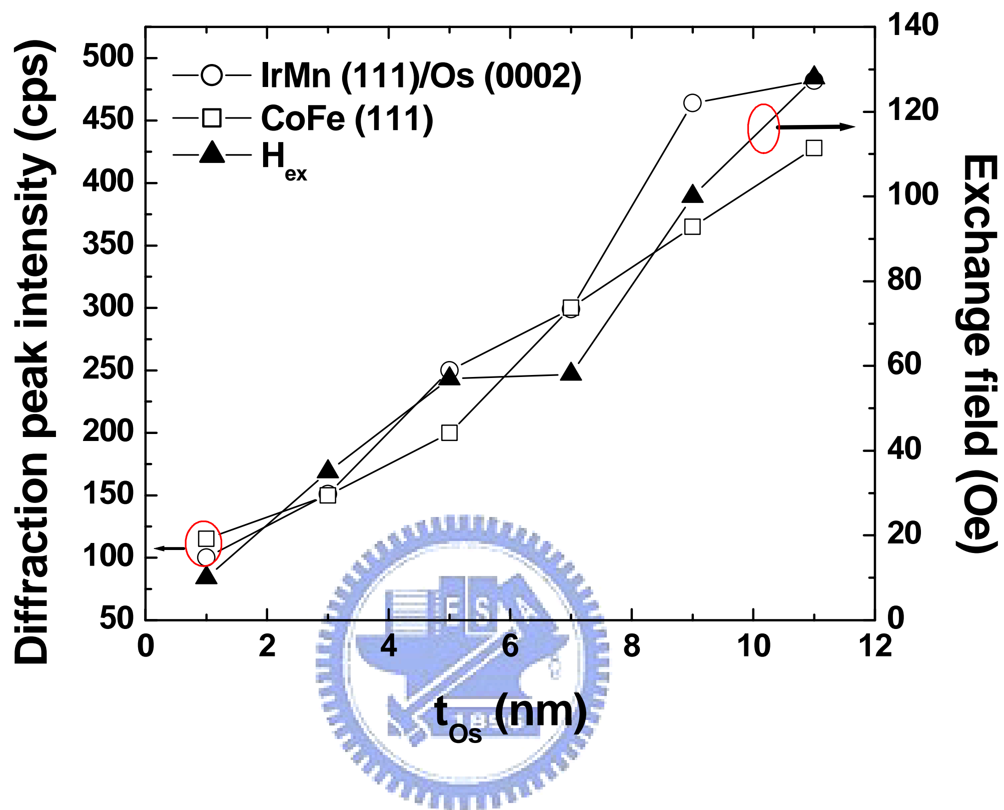

Fig. 4-20 The diffraction peak intensities of the IrMn (111)/Os (0002) and CoFe (111), and H_{ex} varied as a function of the Os buffer thickness.

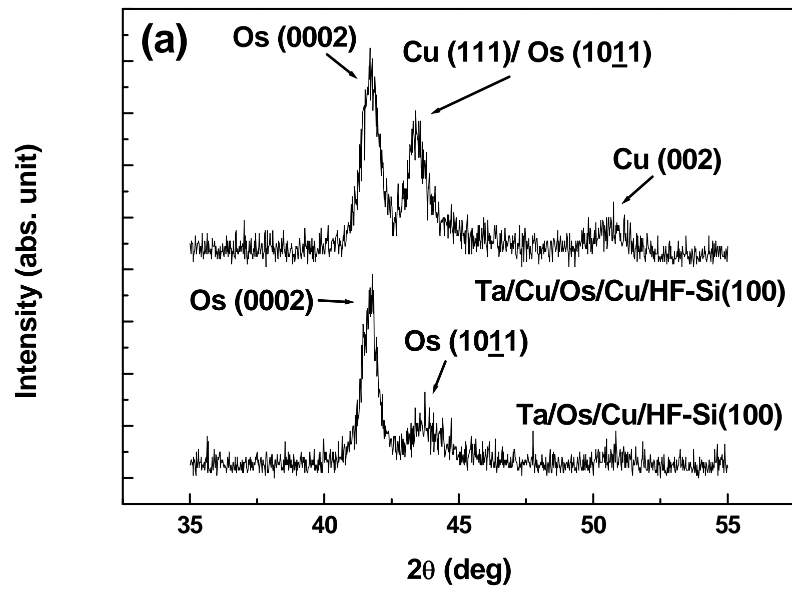

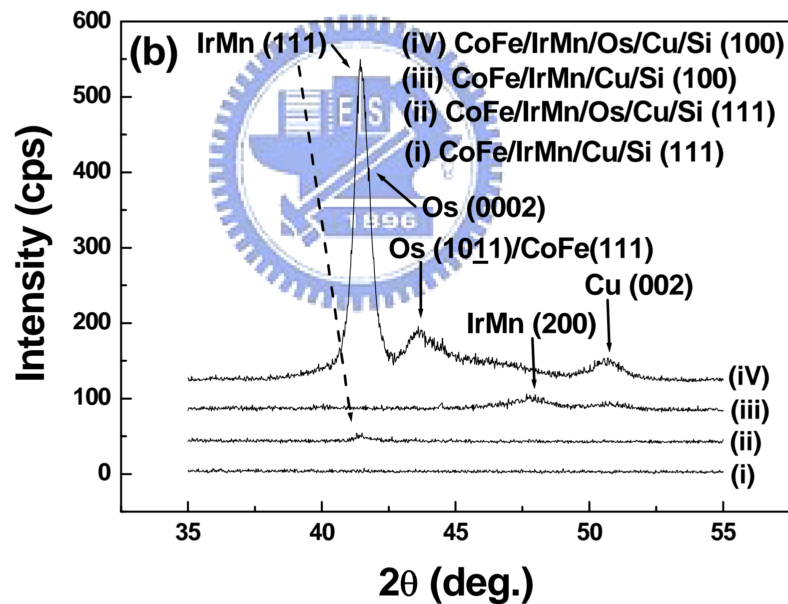

Fig. 4-21 (a) XRD patterns of the evidence that the Os (0002) can provide a suitable surface mesh to grow fcc (111) orientation. (b) XRD pattern of CoFe/IrMn grown on Cu/H-Si (100) and Cu/H-Si (111) with and without Os buffer layer.

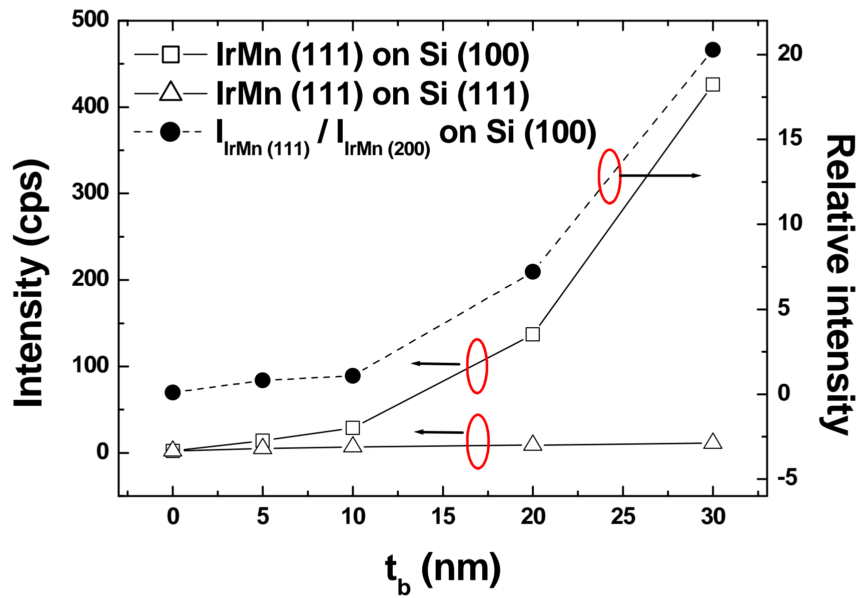

Fig. 4-22 The $I_{IrMn\,(111)}$ on Si (100) and Si (111) and the relative intensity of $I_{IrMn\,(111)}$ / $I_{IrMn\,(200)}$ were a function of t_b.

ES 1896

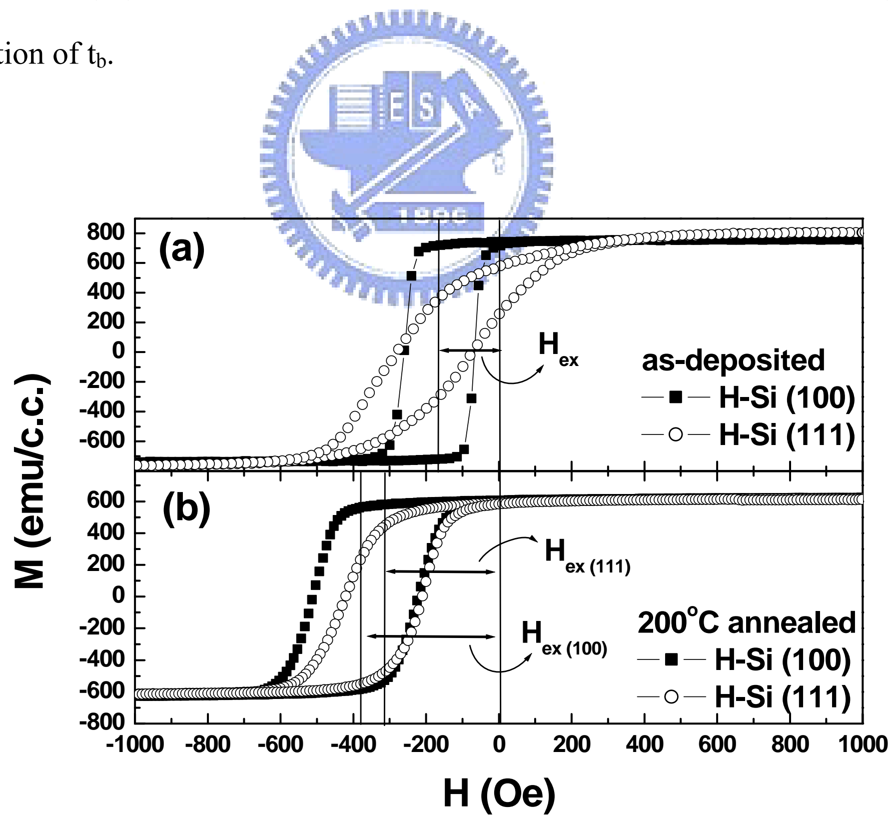

Fig. 4-23 The M-H loop of as deposited (a) and 200°C annealed (b) of CoFe/IrMn/Os30/Cu on both H-Si (100) and H-Si (111) substrates with Os buffer layer.

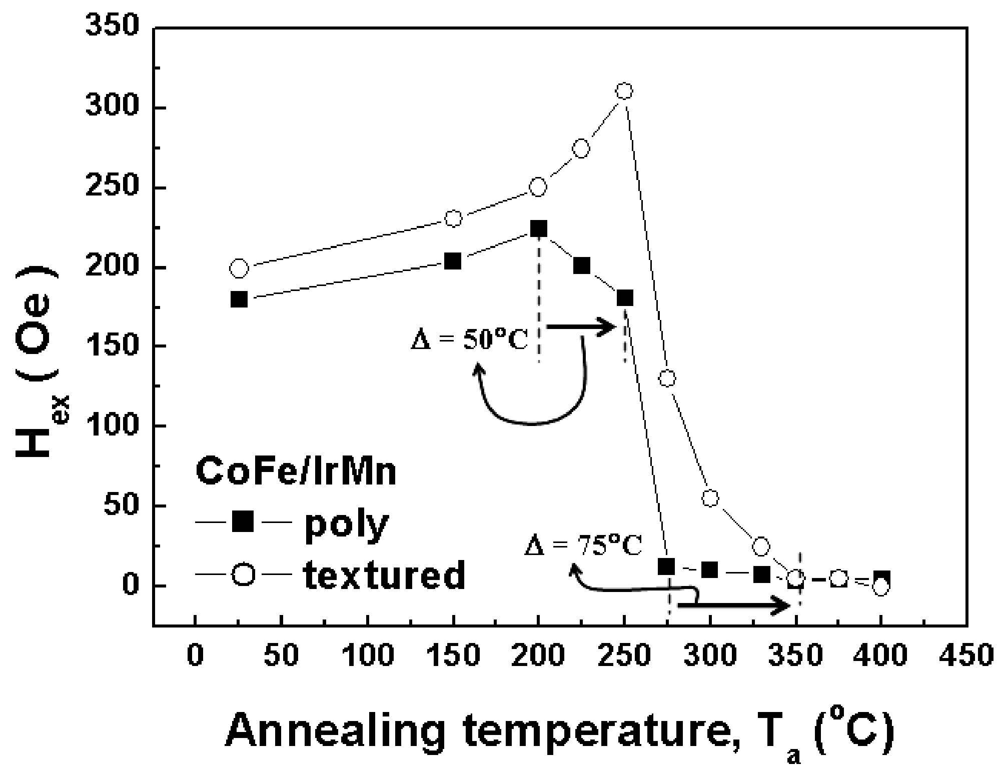

Fig. 4-24 The H_{ex} of the textured and poly-crystalline (poly) samples is as a function of T_a. The textured CoFe/IrMn film showed better thermal stability than the poly sample. The 50°C and 75°C of improvements on the temperature of obtaining the $H_{ex,\ max}$ and the H_{ex} disappearing were found clearly.

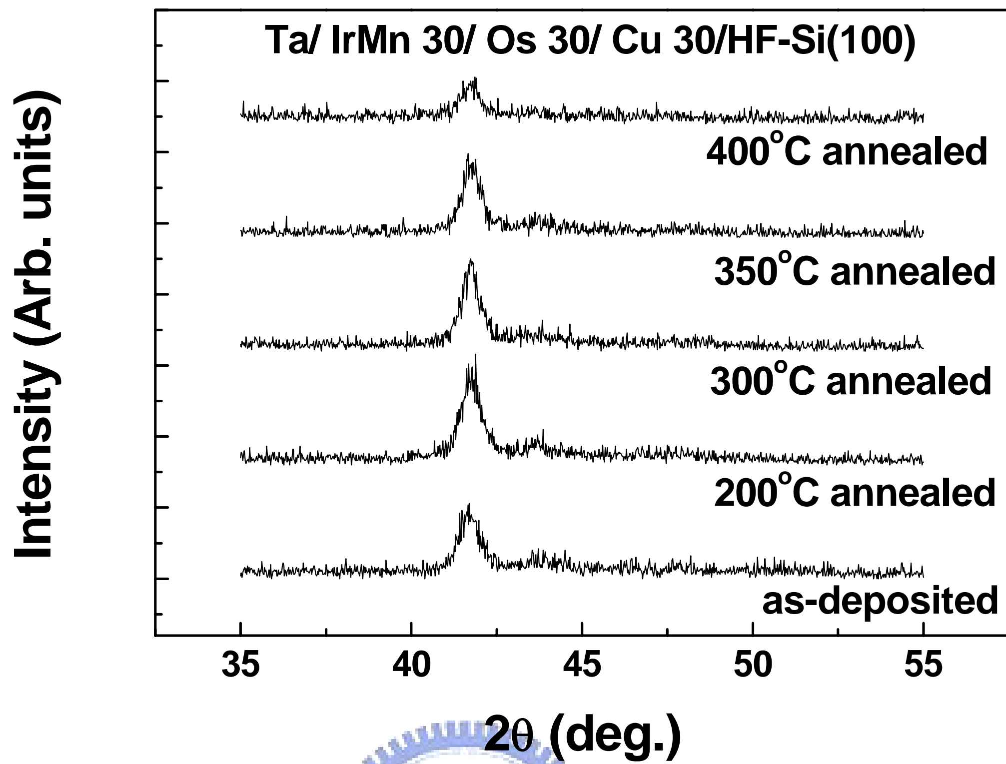

Fig. 4-25 The XRD results of the textured IrMn film grown on Os/Cu buffer layer as T_a increased and only a small destruction of IrMn film structure is found when T_a = 400°C.

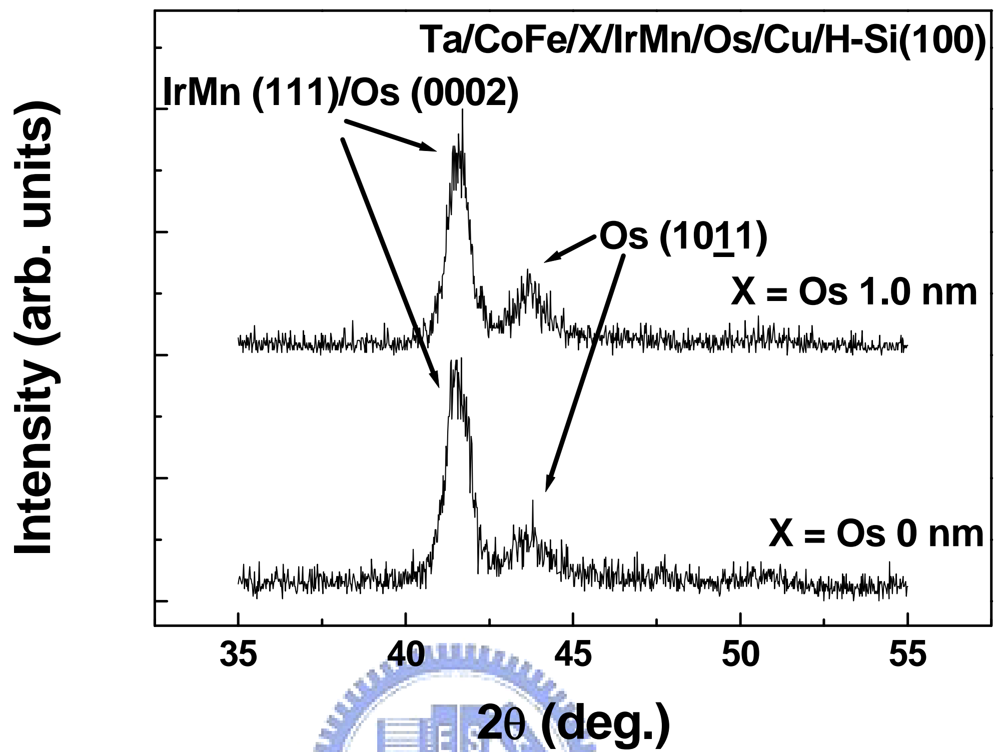

Fig. 4-26 The XRD results of the textured CoFe/IrMn with and without the Os insertion layer in the interface. Such a thin inserted Os layer does not affect the film structure.

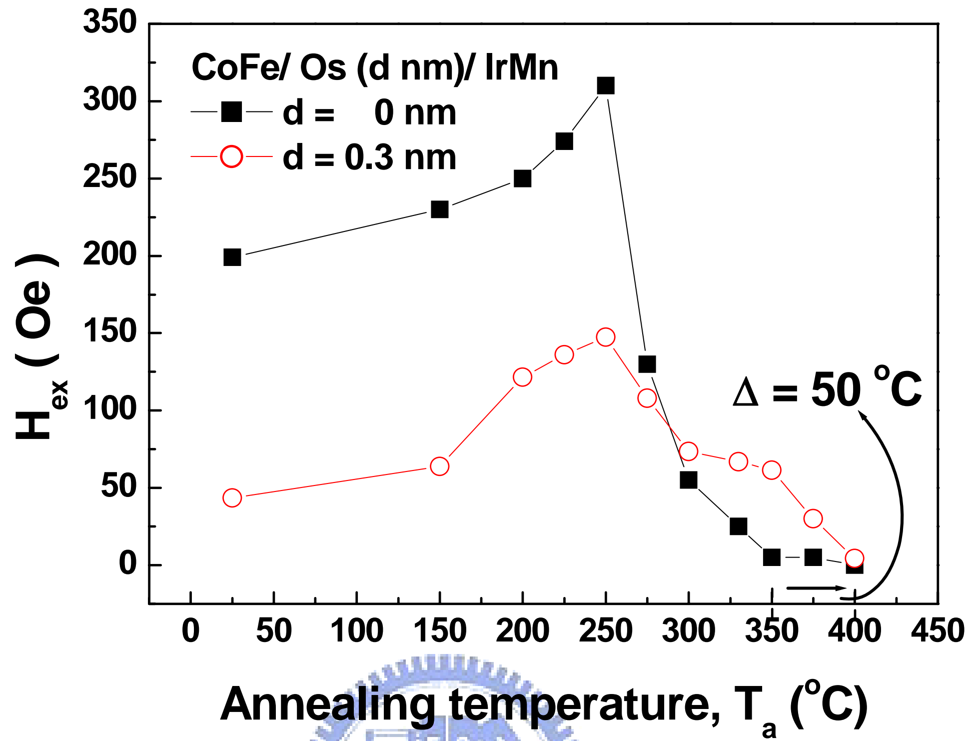

Fig. 4-27 The H_{ex} of the textured samples with different d is as a function of T_a. The 0.3 nm Os inserted textured CoFe/IrMn film showed better thermal stability than the textured one without d. It is clearly found that the 50°C improvement on the temperature, at which the H_{ex} disappearing.

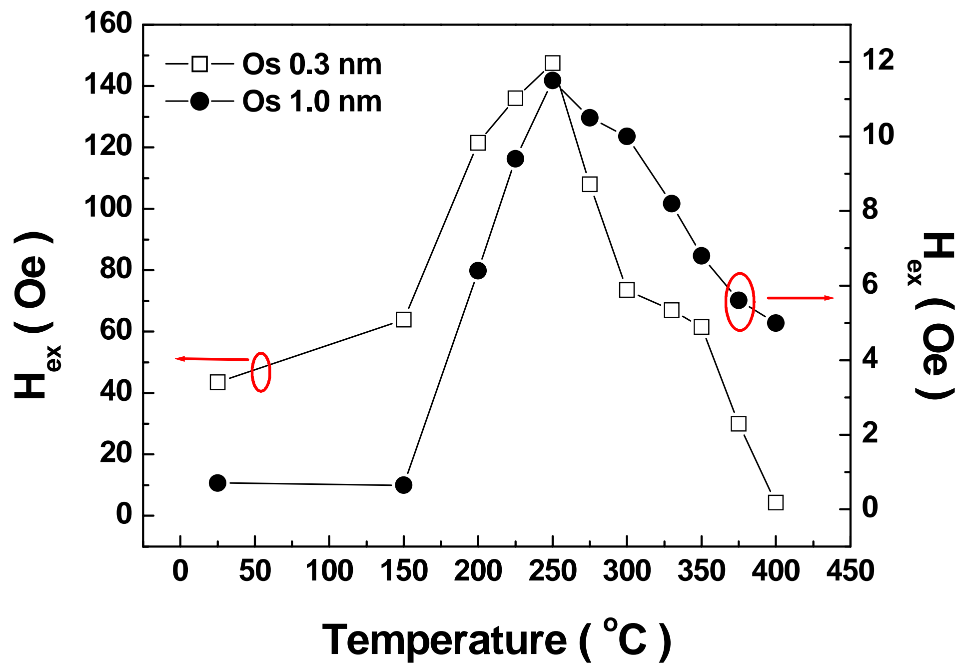

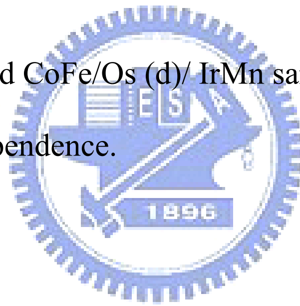

Fig. 4-28 The H_{ex} of the textured CoFe/Os (d)/ IrMn samples with d = 0.3 nm and d = 1.0 nm showed similar temperature dependence.

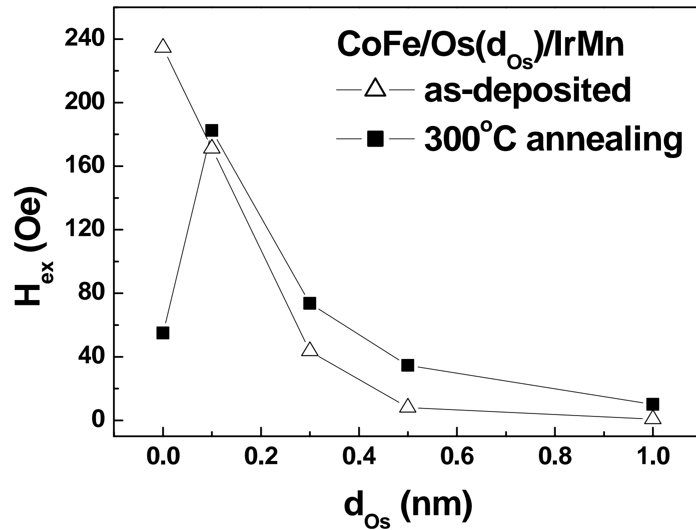

Fig. 4-29 The H_{ex} of the textured sample is as a function of d. A thin Os barrier in the interface of the CoFe/IrMn made it more stable at high temperature. When d > 0, the all samples with T_a = 300°C showed larger H_{ex} than that of as-deposited state, while the H_{ex} of the sample without d = 0 nm degraded sharply.

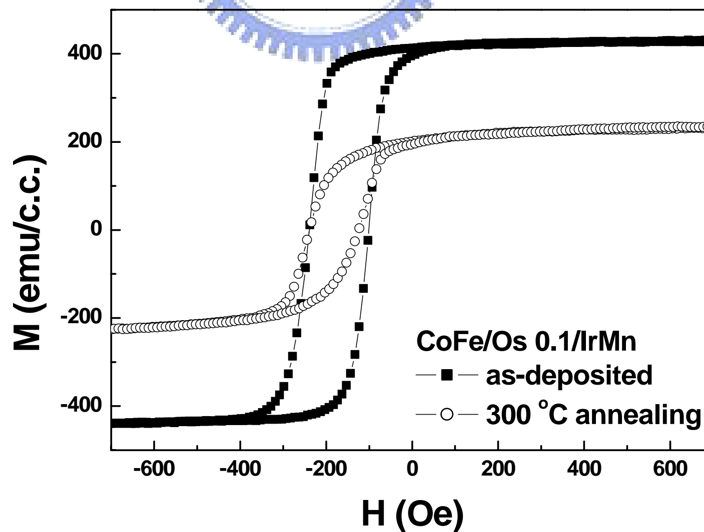

Fig. 4-30 The Hysteresis loop of the CoFe/Os 0.1/IrMn textured sample. The whole magnetic behavior was almost the same before and after 300°C annealing. Only half reducing of magnetic moments and a little rising of H_{ex} were found.

4-2-2 Growth of Os (0002) on different substrates

The non-volatile memory, MRAM, has attracted many attentions due to its high speed, high density, and radiation-resistive properties. For high density products manufacturing, it is required to combine the MTJ, which is the basic cell unit of MRAM, and ultra large scale integration (ULSI) processes. Some of the factors affecting the whole performances of MTJ are the crystallinity of the memory cell and the thermal diffusion issues. Many kinds of seed layers were used for growing memory cell with crystalline structure on Cu to simulate the actual case during manufacturing. However, the high temperature process will cause thermal diffusion of Cu, and the MTJ will get worse once that occurred[1]. Very few epitaxial seed layers grown on Cu metal line were studied for growing crystalline magnetic films. Furthermore, with a Cu (002) film prepared by MMES method, some face-center cubic (fcc) metals, such as Ni, Pd, Co, etc., can be grown along their own [001] direction [103]. Some metal with larger lattice mismatch relative to the Cu/Si can also grow with other inserted seed layer between the metal and Cu [100]. However, there are fewer papers reported on the growth of the hexagonal closed packed (hcp) metal [129], especially no any reports related to the Osmium noble metal. Recently, pure osmium (Os) film was suggested to be a good glue layer and a barrier layer for Cu interconnections in Damascene processes [14, 99]. Previous section showed that the Os was a good buffer effort on enhancement of the magnetic property of magnetic films on SiO_2. In this section, the high (0002) orientated and epitaxial (0002) Os films prepared on different substrates by magnetron sputtering deposition were systematically studied.

Samples with the structure of Os (t_{Os})/ (Cu t_{Cu})/ (Au, Ag, and Pd 10) on Si substrates were deposited by physical vapor deposition (PVD) method, where the thickness was in nm. The Os and Cu were grown by standard magnetron sputtering, and Au, Ag, and Pd were

deposited by e-beam evaporation. Before depositions, all Si wafers were first cleaned by using acetone to degrease and dip into 10% HF solution for several seconds to form a hydrogen-terminated surface, and then loaded into the vacuum chamber immediately. Base on the MMES technique [130], the Cu film grown on Si (100) showed high (002) orientation [108, 131]. The 12-fold symmetric Os film was epitaxially grown on Si (100) substrate with a Cu seed layer, and the Cu and Os films were deposited in sequence at about a 5 mTorr pressure of pure Ar gas without breaking the vacuum. No external heating was applied to the substrates during films growth. On the other hand, in the case of 6-fold symmetric Os film growth, the Si (111) was used, and one of the Au and Ag was deposited first. Then, the samples were sent to the sputtering system as soon as possible, and the deposition conditions of the Os and Cu were the same with that of the case of 12-fold symmetric Os film growth. To verify the in-plane orientation relationships between layers, asymmetric in-plane φ scans were carried out.

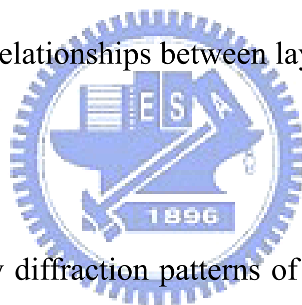

Fig. 4-31 shows the X-ray diffraction patterns of as-deposited 30 nm Cu and 30 nm Os films with and without 30 nm Cu seed layer on H-Si (100), respectively. Not only the atomic arrangement of the H-Si (100) surface mesh is much different to that of Os (0002), but also the minimum lattice mismatch between Os and H-Si (100) is near 30% (with a 45°-rotation of the Os (0002) plane around Si [001]). Thus, Os can not grow as an oriented film directly on H-Si (100), and this can be further proven by the observation of two weak diffraction peaks, Os $(10\bar{1}1)$ ($2\theta = 43.67°$) and Os (0002) ($2\theta = 41.69°$). However, Cu with a lattice constant of 3.62 Å can reduce the lattice mismatch to 5.5% by a 45°-rotation of the Cu (002) plane around Si [001], and thus Cu can grow with a weak 4-fold symmetry on H-Si (100). The lattice mismatch for Os-Cu was only 7.2% when there is a 45°-rotation of the Os (0002) plane around its [0002] axis during film growth. This well-improved lattice match makes the Os grown with a high [0002] prefer orientation and parallel to the [002] direction of the Cu seed

layer, which is perpendicular to the substrate surface. It is noted that the mismatch is not small enough, which is likely one of the reasons for the observation of the $(10\underline{1}1)$ peak of the Os film grown on Cu. As the thickness of the Os film increasing, the Os (0002) peak intensity was raised clearly, as shown in the inserted picture in Fig. 4-31 for 100 nm Os film. As the Os (0002) peak intensity increasing, the peak position was found to slightly shift to lower angle; this is resulted in the stress induced from the mismatch of the Os and Cu interface.

The TEM cross sectional images of the Os film are shown in figure 4-32 (a). Although the TEM cross section images of the Os film showed slightly rough interface between Os/Cu, and did not reveal clear crystal structure. However, many areas do exhibit clearly layer by layer structure, as shown in Fig. 4-32 (b). The interface between Cu and Os was obviously found to exist continue layer structure. It indicated such areas showed a good layer by layer growth for both Cu and Os films. As shown in Fig. 4-32 (c), the growth direction of Os (0002) plane is perpendicular to the interface. Figure 4-30 shows the X-ray diffraction pattern of the Os film with the thickness of Cu buffer layer varied from 1 to 30 nm. The crystal structure of the Os layer is dependent on the thickness of the Cu seed layer. At an initial growth stage, the Cu_3Si silicide is formed [132], therefore, the Os $(10\underline{1}1)$ peak did not appear when the thickness of the Cu seed layer was less than 10 nm. This means the Cu-Si silicide did not provide a suitable surface to grow the $(10\underline{1}1)$ orientation of Os film. The intensities of the Os (0002) peak have a proportional dependence on the Cu thickness.

In general for a hcp structure, if the film is (0002) epitaxial growth with a single in-plane orientation, only six normal directions of equivalent $\{10\underline{1}1\}$ type planes lie on the surface of the cone with the angle of 61.957° from the [0002] film normal. The φ scan of the Os film on Si (100) is shown in Fig. 4-34 (a). A twelve Os $\{10\underline{1}1\}$ peaks separated by 30° were observed, and indicated a 12-fold in-plane symmetric structure. It implied that the in-plane orientation

of Os was not totally random. According to the θ-2θ scan and the φ scan results, the orientation relationships between the first Cu layer and Os layer can be determined, as schematically illustrated in Fig. 4-34 (b). Two sets of (0002) epitaxial grain (marked as "A" and "B" grains) rotated by 90° with respect to each other along [0002] direction were formed in the Os layer. The relationships are: Cu(002)//Os(0002), Cu[$1\underline{1}0$]//Os[$11\underline{2}0$], Cu[110]//Os[$2\underline{1}10$] in "A" grain, and Cu(002)//Os(0002), Cu[$\underline{1}\underline{1}0$]//Os[$11\underline{2}0$], Cu[$1\underline{1}0$]//Os[$12\underline{3}0$] in "B" grain. Therefore, such an Os film showed a 12-fold in-plane symmetry from the twin relationship of the different 6-fold symmetric grains. Similar structures were found in Pd film on MgO (001) [133] and Au on Cu (002) [134]. There are some transitional areas existing between these two sets of grains. This may be suitable for other Os atoms to form different plane, and the Os ($10\underline{1}1$) peak was experimentally observed.

However, with the same growth conditions, the Os film did not grow epitaxially on the Si (111) surface. Figure 4-35 (a) shows the TEM cross section images of the Ta/ Os 25/ Cu 10/ Si (111). That the 200 nm Cu layer did not shown good (111) crystalline structure on Si (111) by the MMES method [130], and, indeed, a 100 nm Cu layer showed weak Cu (111) diffraction was reported [135]. The 10 nm Cu was too thin to form good crystalline structure on Si (111). The non-smooth interface (as shown by the white dash line in fig. 4-35 (b)) was easily found, and thus the Os (0002) grown along different direction (as shown by the white arrows in fig. 4-35 (b)). The φ scan of the Os {$10\underline{1}1$} of the Os on Si (111) showed random in-plane orientation, as shown in fig 4-35 (c). No symmetry was observed when Os film grown on Si (111) with a Cu seed layer.

The mismatch of Os/Pd (~2.4%) was small; however, as seen from Fig. 4-36 (a), the Os on Pd/Si (111) formed very highly (0002) orientation. Nevertheless, the Pd grown on H-Si (111)-1x1 did not form epitaxial film as revealed from XRD φ scan shown in the inset in Fig.

4-36 (a). Furthermore, these results meant the Pd on H-Si (111)-1x1 was locally formed fcc (111) surface, which is suitable for Os (0002) growth, while these local areas were totally random distribution in the surface plane. The Pd also shows solubility in Os-base binary phase diagram [121]. Some Pd-Si intermixing region was found in the TEM image. Moreover, most areas of Pd layer showed very clearly atomically arrangement, while some dislocations appeared in the interface between Pd and Os tilted the Os growth direction, as shown in Fig. 4-36 (b). Thus, the Os grew without any in-plane symmetry even the mismatch was relatively small and the Os grown on Pd was only showed highly textured behavior instead of epitaxial behavior. This implied that the surface state is a key factor to grown the epitaxial Os film. Indeed, according to the past studies, only Pd_2Si (111) epitaxially grown on Si (111) could be found after 200~700°C annealing [136]. In some samples, the Os grown on such a Pd-buffered substrates showed poor adhesion. That may be another reason why Os film can not epitaxially grow on H-Si (111) with Pd buffer layer.

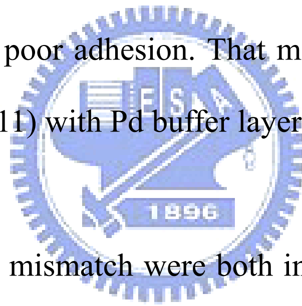

Surface energy and lattice mismatch were both influenced the Os epitaxial film growth. For instance, Os grown directly on H-Si(111)-1x1 only showed two weak diffraction peaks relative to Os (0002) and Os (10$\underline{1}$1) due to the large mismatch (> 30 %) and the large surface energy (4.57 J/m^2) [137]. Although the Cu had lower lattice mismatch with Os (0002) (~ 6 %), the larger surface energy (1.95 J/m^2) and the lattice mismatch with H-Si (111)-1x1 (~ 10 %) made it hard to grown on H-Si (111)-1x1 epitaxially to form fcc (111). Thus, the Os on such a surface still showed neither strong diffraction Os (0002) peak nor in-plane symmetry. The body center cubic (bcc) type transition metal had not been reported to grow epitaxially on H-Si (111)-1x1. Due to the H-Si (111)-1x1 having the fcc (111) (1x1) terminated surface and a geometric model of the coincidence-site lattice [138] of Ag on the H- Si (111) surface suggested that the epitaxial growth occurred when it meets the condition: $4*a_X = 3*a_{Si}$. Thus, the metal grown epitaxially on it must have the same atomic arrangement, i.e. fcc (111) or hcp

(0002) arrangement, to restrain the surface energy. That is the reasons the fcc metals were selected in this study. The 6-fold symmetric Os film was successfully grown on Si (111) with Au buffer layer. As shown in Fig. 4-37 (a), the XRD pattern indicates the clearly Os (0002) peak and Au (111) peak at 41.69° and 38.18°, respectively. Since Au grown on hydrogen-terminated Si (111) surface (H-Si (111)-1x1) provided a perfect fcc (111) surface mesh, the Os was (0002) oriented epitaxially grown due to the lower mismatch (~7.9 %) in the lateral nearest distance between atoms, while the hcp (0002) has similar atomic arrangement with the fcc (111). The six Os {10$\underline{1}$1} peaks were revealed from the XRD φ scan results and shown in the inset in Fig. 4-37 (a). This indicated good crystalline structure Os with 6-fold symmetry was obtained. Besides, Ag was selected to be the better buffer layer for growing the epitaxial Os film due to the lowest surface energy (1.17 J/m^2) and the low lattice mismatch (~7.4%) compared with H-Si (111)-1x1. Figure 4-34 (b) shows the XRD pattern of the epitaxially Os film grown on Ag/H-Si (111)-1x1. Both the Os (0002) and Os (0004) (near 90°) peaks were observed indicated the good crystalline structure. The strong Os (0002) peak and the obvious 6-fold symmetry as revealed by XRD φ scan, shown in the inset in Fig. 4-37 (b), also implied the Os film was epitaxially growth. For all epitaxial samples, Os showed identical φ scan spectra of those of buffer layers (Au and Ag), indicating that the cubic-to-cubic in-plane epitaxial relationship between Os and Ag (or Au) were existed. Furthermore, once the perfect fcc (111) plane was formed by Au (or Ag) on H-Si (111)-1x1, another inserted Cu between Au (or Ag) and Os did not affect the epitaxial growth properties of Os. Figure 4-38 shows the XRD measurements of Os grown H-Si (111)-1x1 with Cu/Ag and Cu/Au buffer layer, respectively. The clear 6-fold symmetry samples were still obtained. It is noticeable that the Cu (111) (near 43°) was obviously found, as shown in Fig. 4-38 (a). This implied again the fcc (111) played in important role for growing the Os (0002) film. As seen from the TEM cross sectional image of the Os/Cu/Au/H-Si (111)-1x1 (Fig. 4-39), the regular crystal structure was found. The epitaxial films did grow well even though the lattice

mismatch between Au and Cu is a little large (~12 %). The atomic layers were grown continuously with some dislocations appeared at the initial stage of the film growth (as seen from the slightly random areas near the center of the image). The inset in Fig. 4-39 identifies the TEM electron diffraction pattern of Os/Cu interface. The clear spots in the electron diffraction pattern were distinguished, and indicated that it was with an epitaxy quality. At the interface, the uniform atomic arrangement is very distinct. That proved the Os epitaxial growth properties.

In addition, some properties of Os are highlighted once more and listed as following: (1) low wetting angle and large adhesive energy for Cu [99]; (2) the melting temperature, electrical resistivity and thermal conductivity are all better than Ta, which is the well used barrier layer in present Damascene trench [14]; and (3) Os can stop Mn diffusion and enhance the CoFe/IrMn fcc (111) crystallinity on Cu/Si (100). Such superior characteristics and the results of this study permitted that the Os have larger potential to apply in the ULSI MRAM process. Since the (111) oriented Cu film can be grown in the Cu metallization process [139], Os can act as a multi-functions material. Os was proposed to be the under layer for Cu metal line or Cu interconnect as both glue and barrier layers. Os can also posit in the MTJ/Cu metal line interface to reduce the Cu interdiffusion into the MTJ sell and, simultaneously, enhance the fcc (111) crystallinity of the magnetic films in MTJ. Thus, Os do have high application potential and play an important role on integrating the ULSI and MTJ processes.

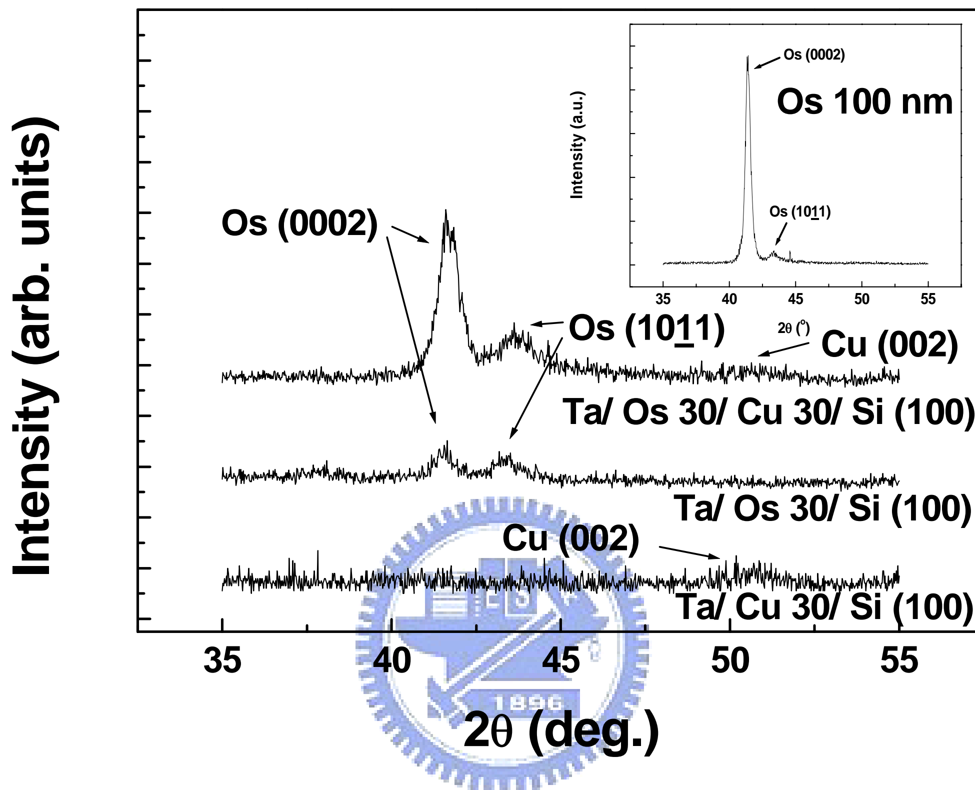

Fig. 4-31 The X-ray diffraction patterns of as-deposited 30 nm Cu film, and 30 nm Os films with and without 30 nm Cu buffer layer on Si(100), respectively. Clear Os (0002) peak and weak Os (10_1_1) peak were observed. The inserted picture shows that the intensity of the Os (0002) was strongly dependent on the thickness of Os layer.

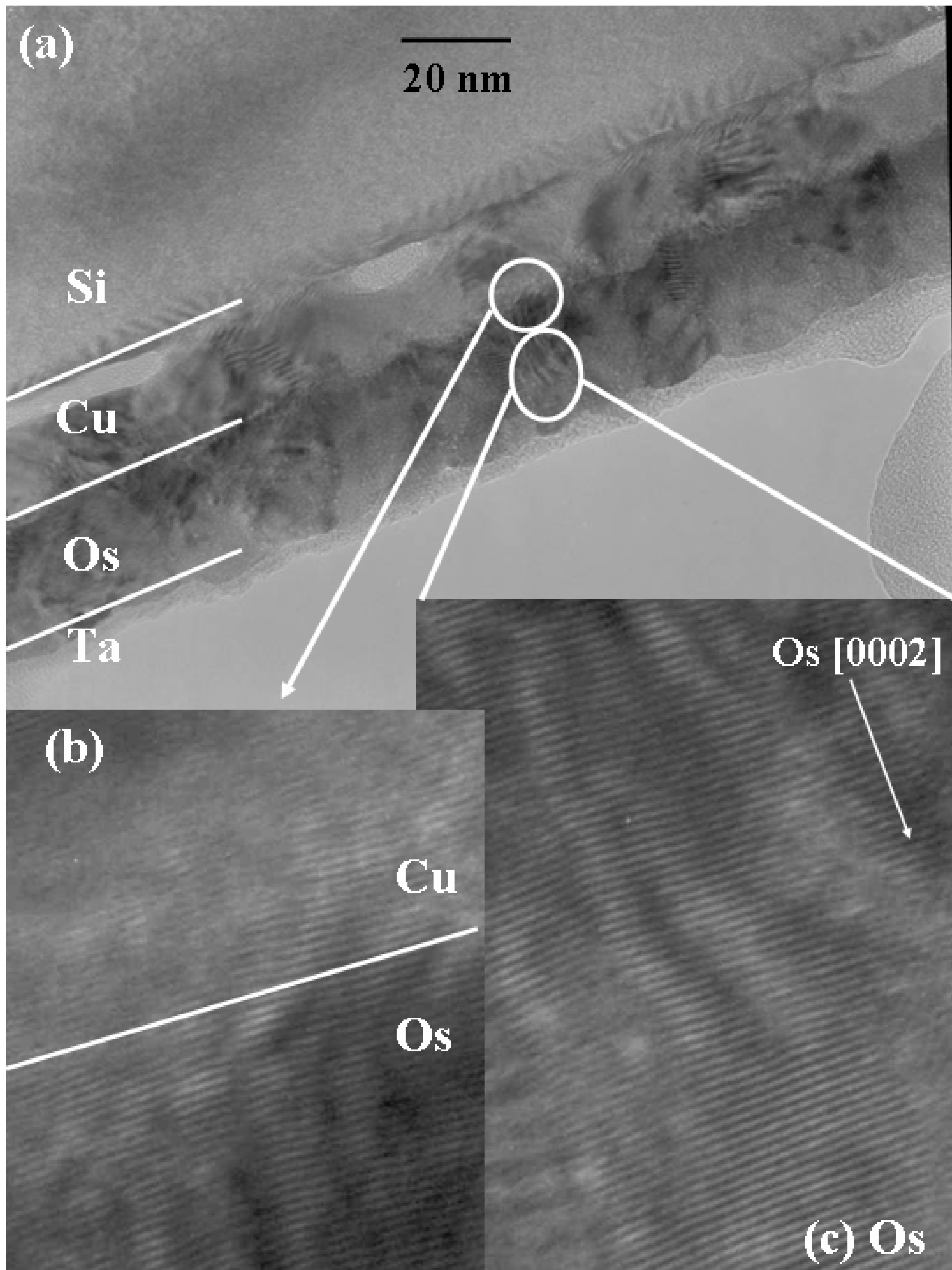

Fig. 4-32 (a) the cross section TEM image of the Ta/ Os 30/ Cu 20/ Si (100). Many areas show very good layer by layer microstructures in the (b) interface between Cu and Os and (c) Os layer.

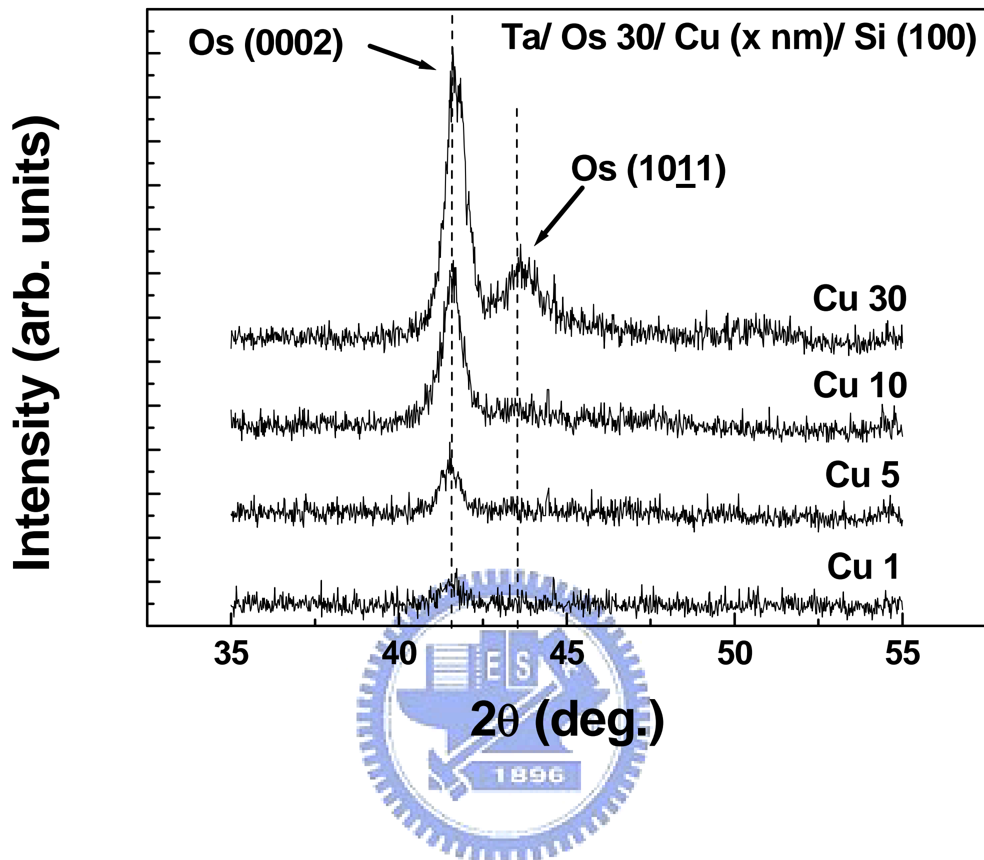

Fig. 4-33 The X-ray diffraction patterns of the Os (0002) peak intensities for samples with the thickness of Cu buffer layer varied from 1 to 30 nm.

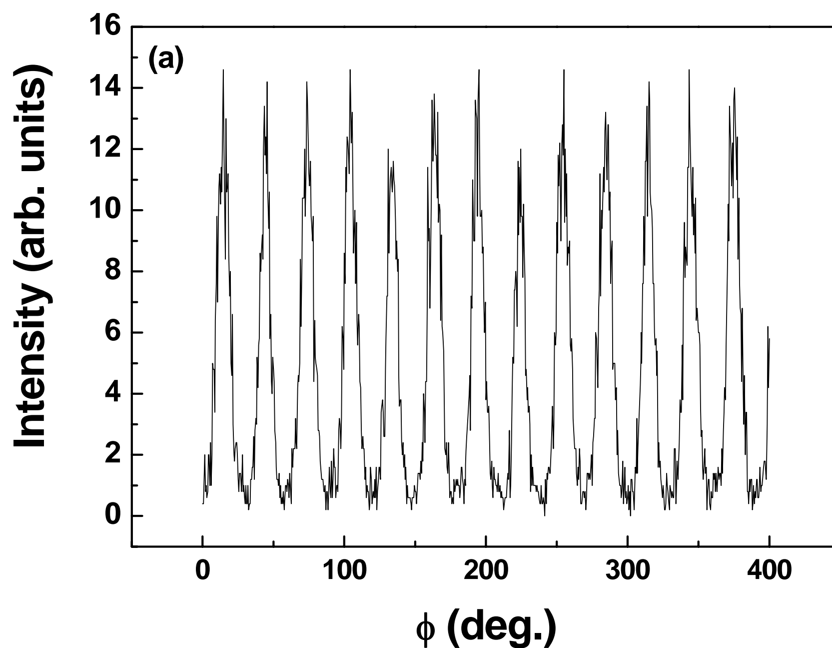

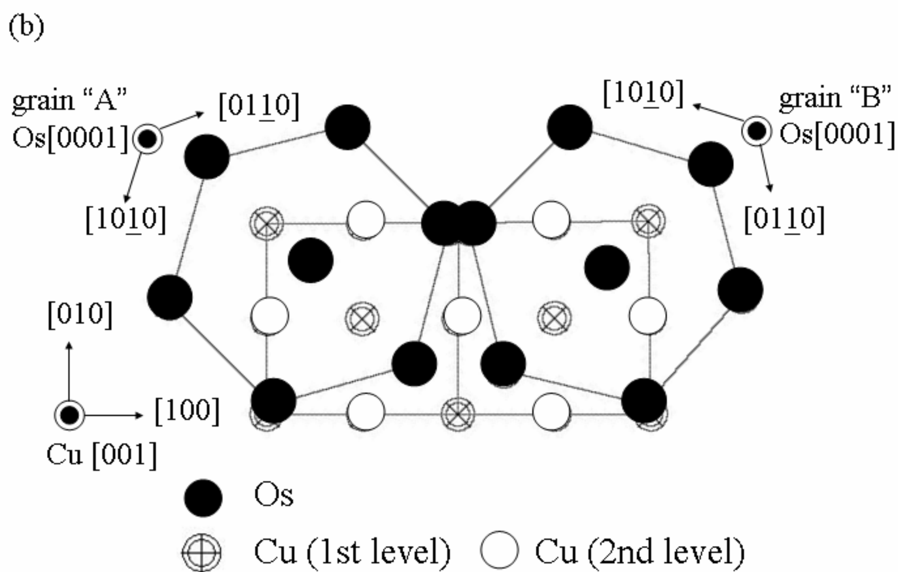

Fig. 4-34 (a) the X-ray φ scans of the Os $\{10\underline{1}1\}$ of the Os on Cu (002)/ Si(100). (b) is a schematic illustration of the epitaxial relationships between Os (0002) and Cu (002). The relationships are: Cu(002)//Os(0002), Cu[$1\underline{1}0$]//Os[$11\underline{2}0$], Cu[110]//Os[$2\underline{1}10$] in “A” grain, and Cu(002)//Os(0002), Cu[$\underline{1}\underline{1}0$]//Os[$11\underline{2}0$], Cu[$1\underline{1}0$]//Os[$12\underline{3}0$] in “B” grain.

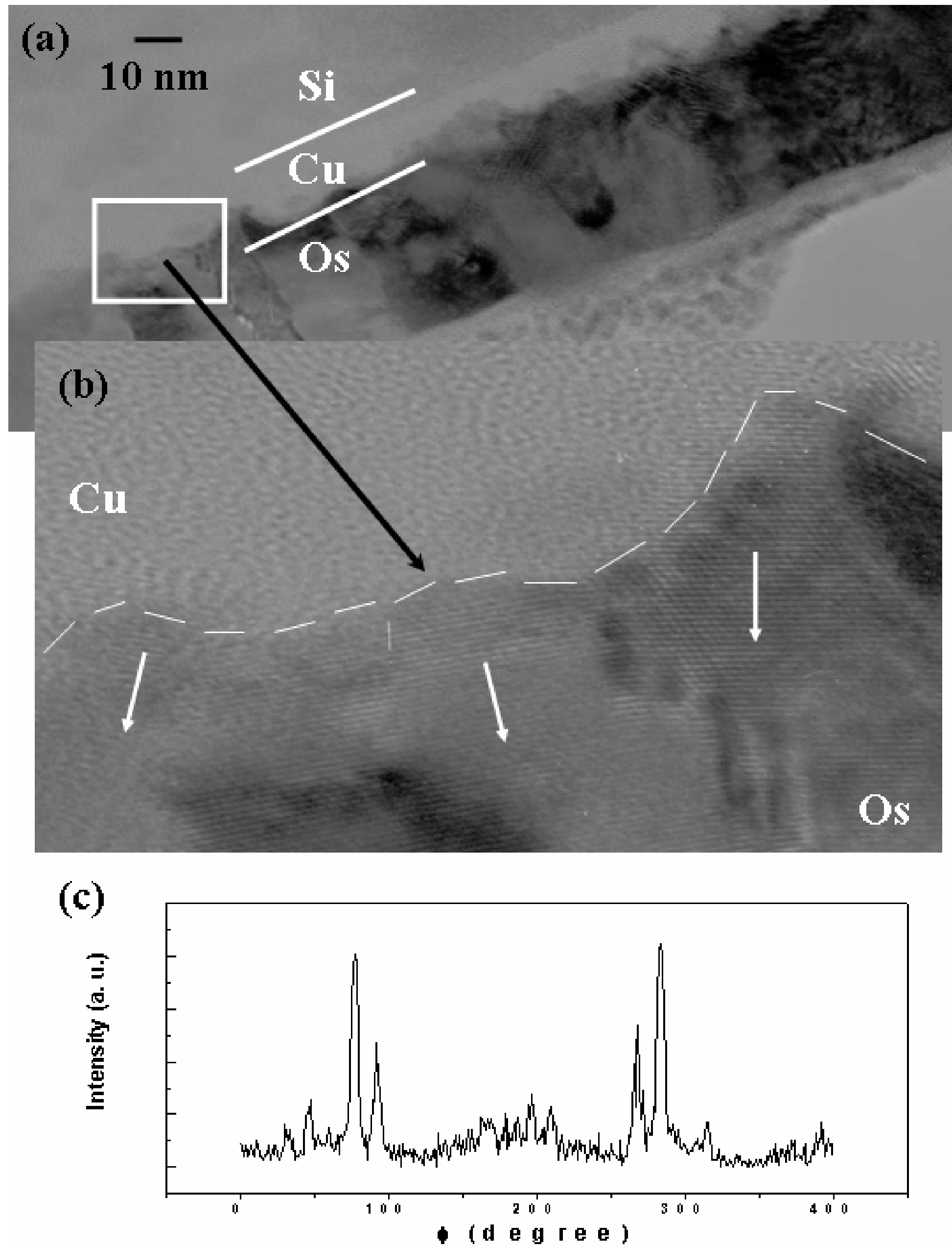

Fig. 4-35 (a) is the cross section TEM image of the Ta/ Os 30/ Cu 10/ Si (111), and (b) is the high magnification view of the interface between Cu and Os layers; while the white dash line roughly presents the non-smooth interface and the white arrows indicate the different growth direction of the Os (0002) near the interface. (c) is the X-ray φ scans of the Os {10$\bar{1}$1} of the Ta/ Os 30/ Cu 10/ Si (111).

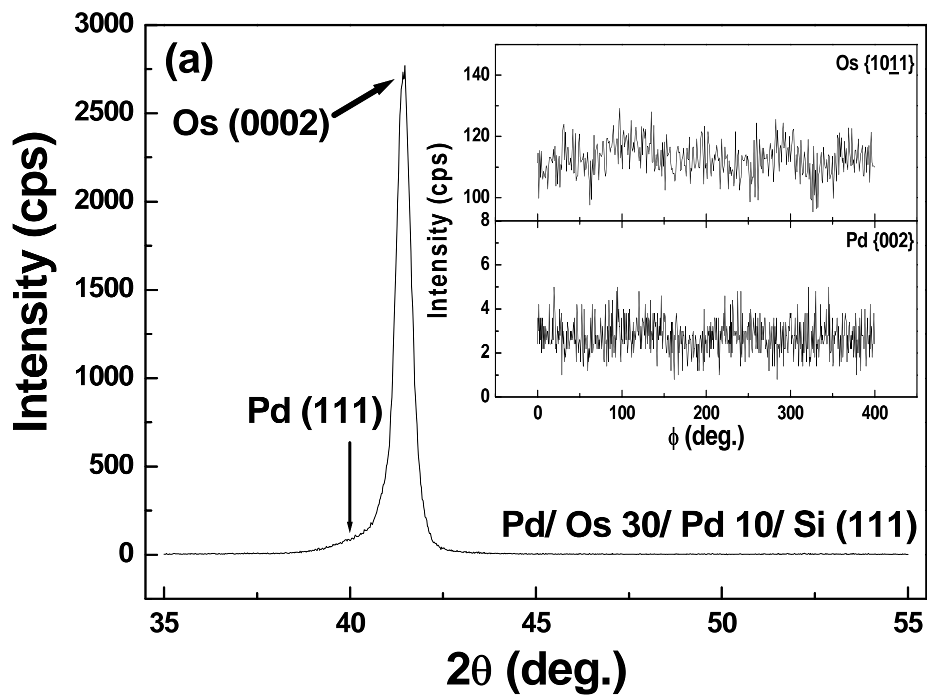

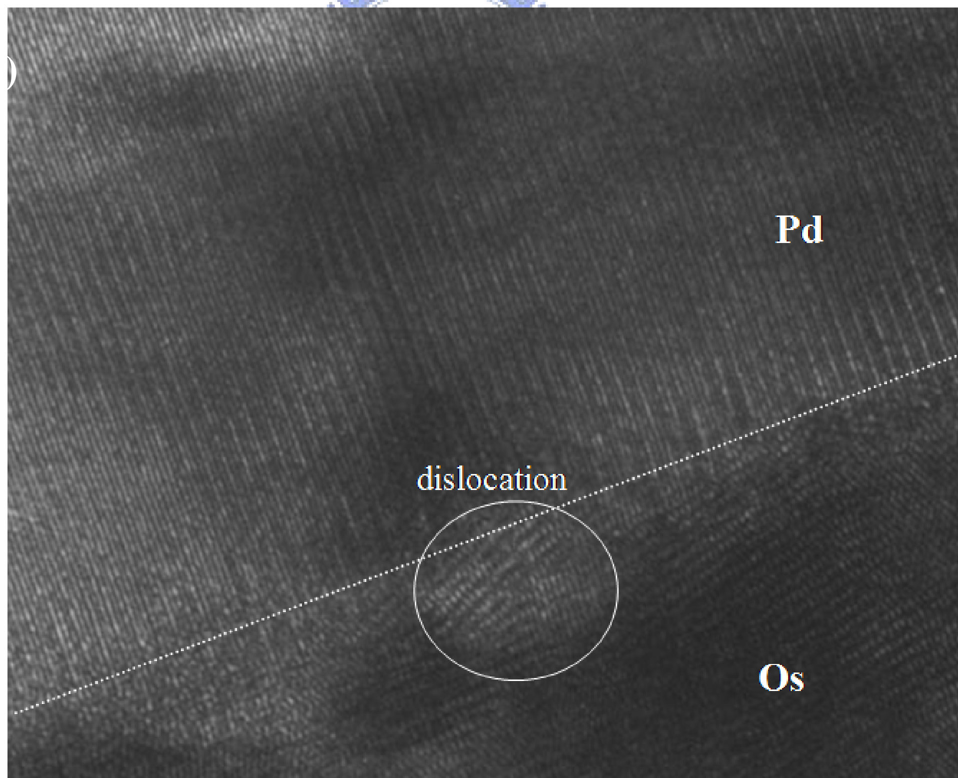

Fig. 4-36 (a) The XRD pattern of Os on H-Si (111) with Pd buffer layer. The inst shows the XRD φ scan results. (b) Some dislocations were found in the cross sectional TEM image between the interface of Pd and Os.

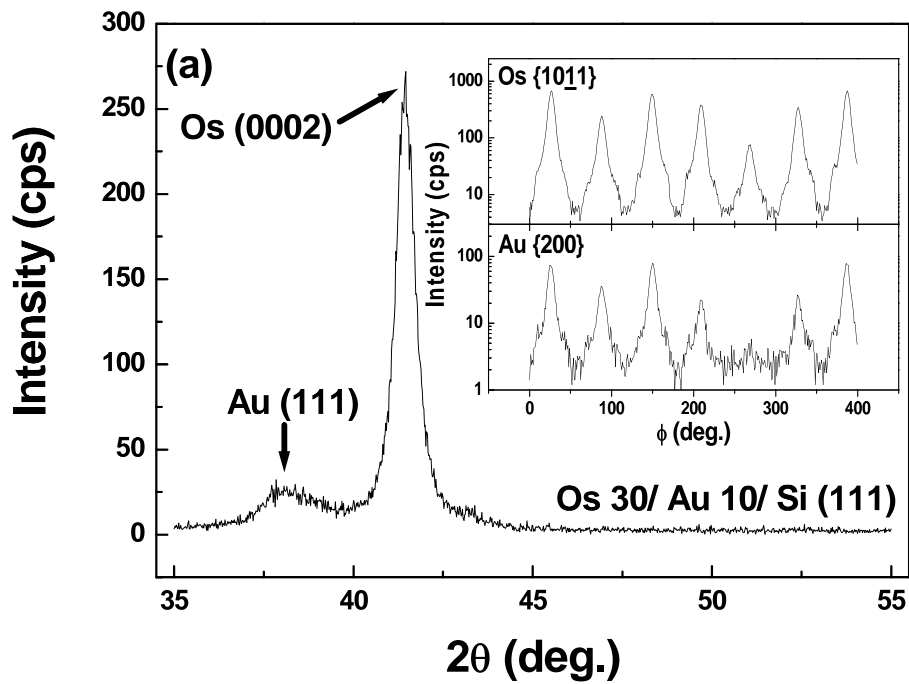

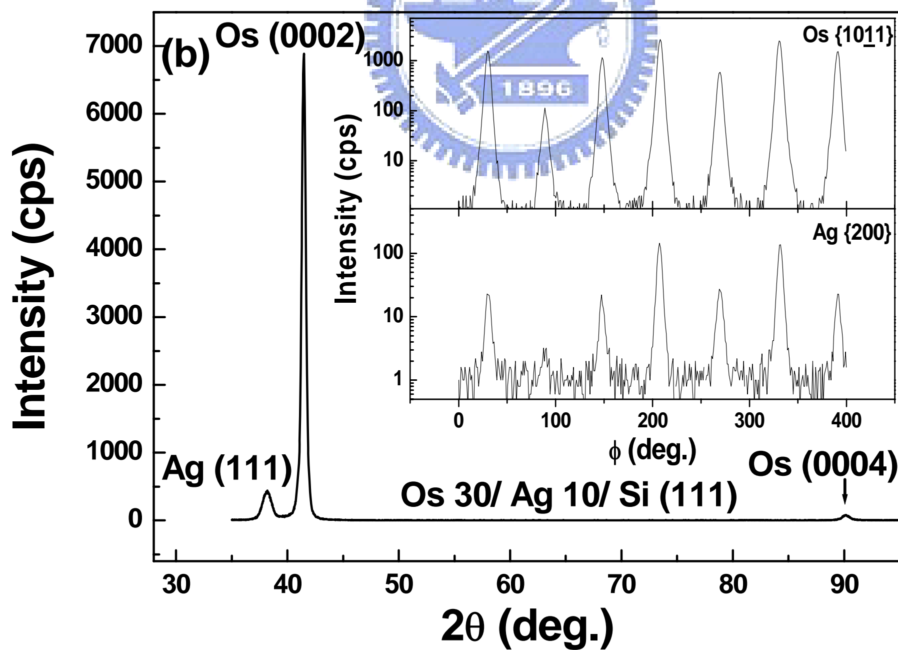

Fig. 4-37 The XRD patterns of Os on (a) Au and (b) Ag buffer layer on Si (111) showed they were both epitaxial growth. The inst in both figures shows the XRD φ scan results, respectively.

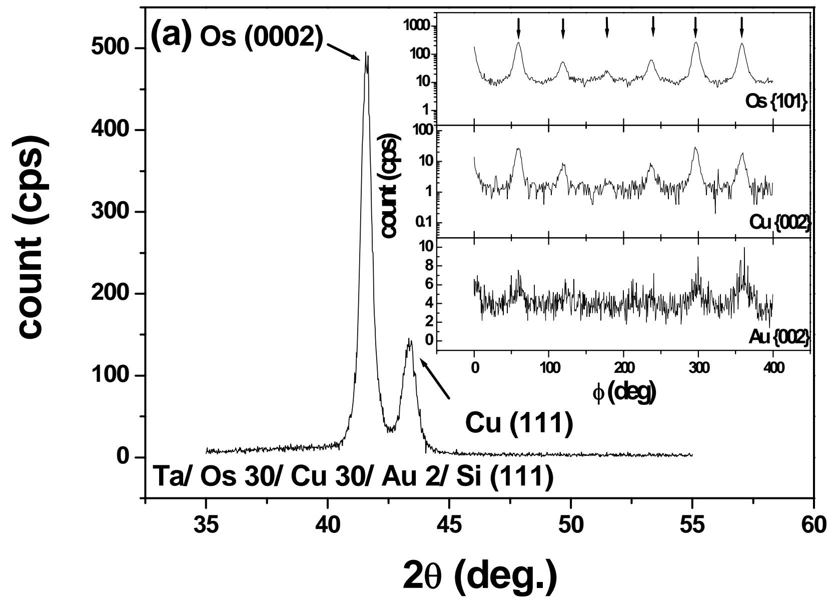

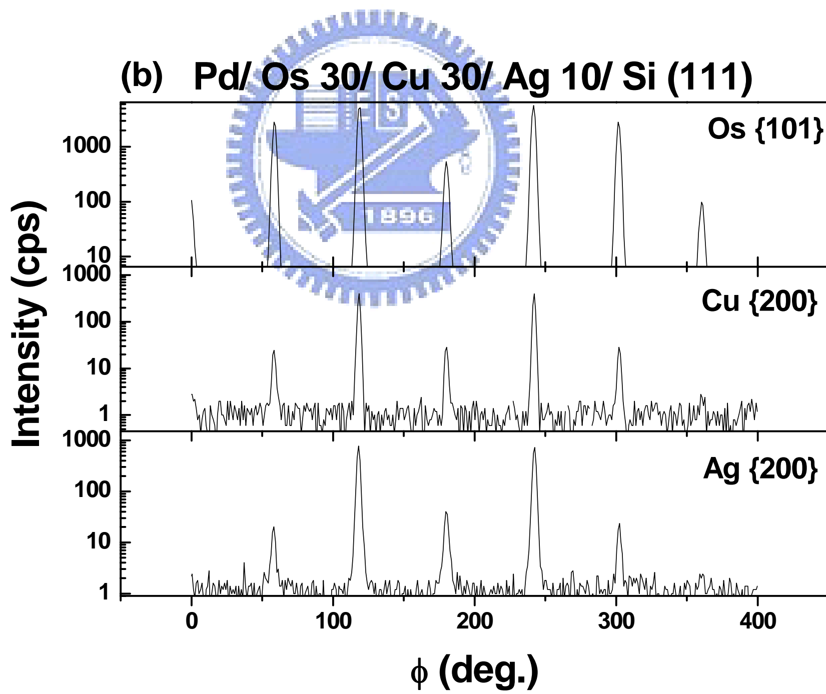

Fig. 4-38 (a) The XRD pattern of Os on H-Si (111) with buffer layer. The XRD φ scan results of Au (the inset in (a)) and (b) Ag both indicated the Os film and the buffer layer were epitaxial growth.

(a)

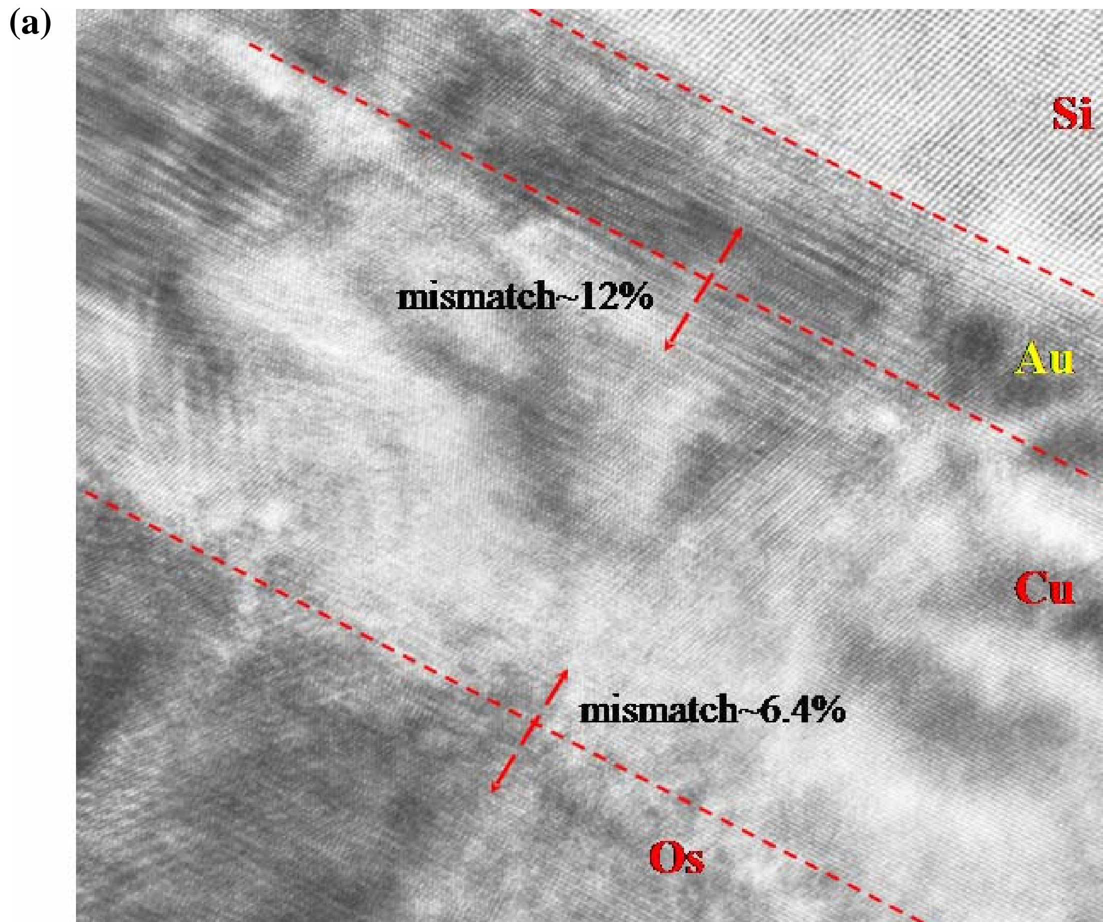

Fig. 4-39 (a) The TEM cross sectional images of Os/Cu/Au/H-Si (111) shows the films growth is closed to epitaxial growth.

(b)

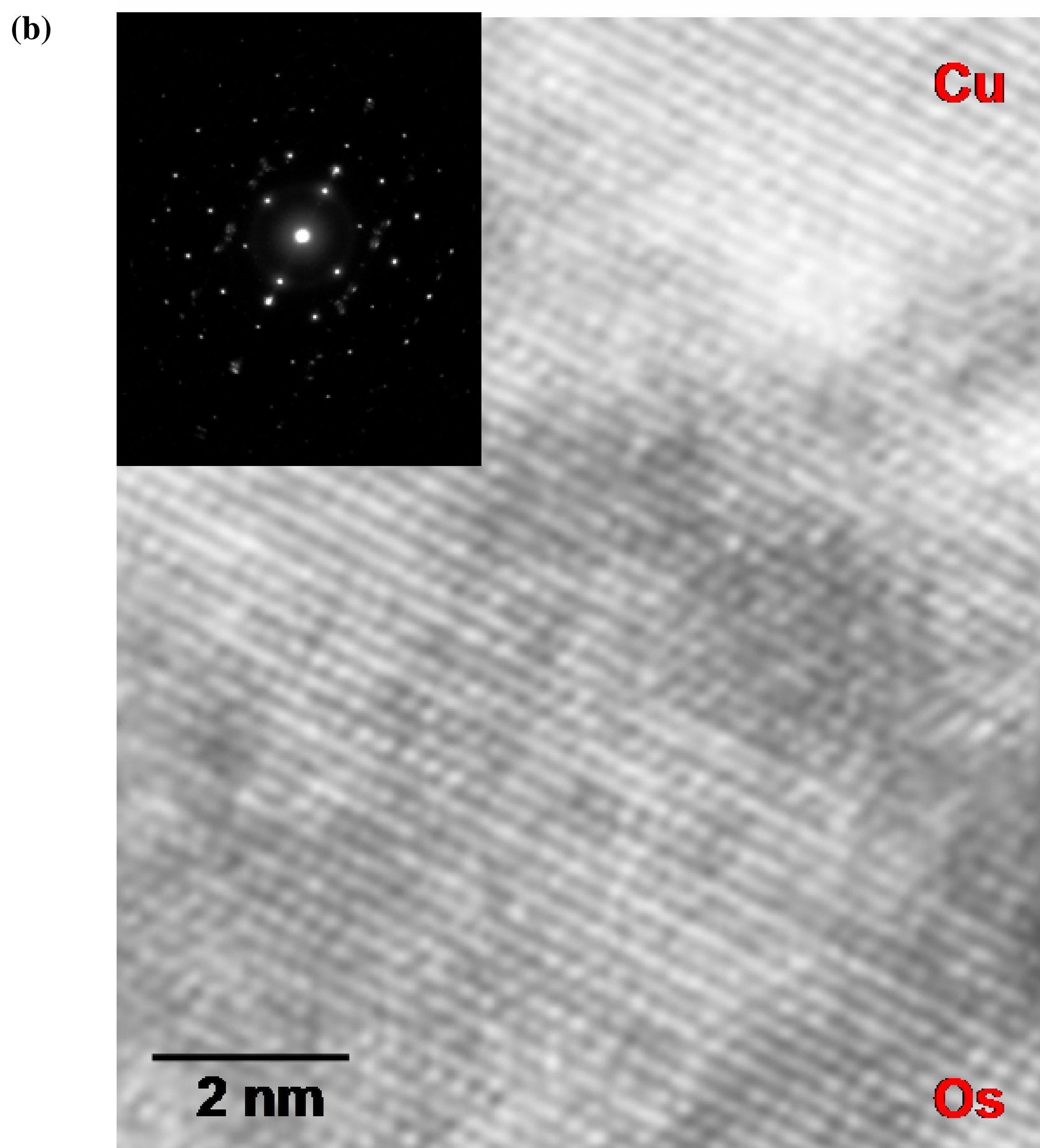

Fig. 4-39 (continued) (b) is the high magnification image of Os/Cu interface and the uniform atomic arrangement can be found. The inset presents the TEM electron diffraction pattern of Os/Cu interface.